The Journal of Chemical Physics ARTICLE scitation.org/journal/jcp

Li diffusion in Si and LiSi: Nuclear quantum effects and anharmonicity

Cite as: J. Chem. Phys. 152, 244101 (2020); doi: 10.1063/5.0007648
Submitted: 14 March 2020 • Accepted: 1 June 2020 •
Published Online: 22 June 2020

Vishank Kumar,[1,a)] Davide Di Stefano,[1] Gian-Marco Rignanese,[1] and Xavier Gonze[1,2,b)]

AFFILIATIONS

[1] Institute for Condensed Matter and Nanosciences, European Theoretical Spectroscopy Facility, Université Catholique de Louvain, Chemin des étoiles 8, B-1348 Louvain-la-Neuve, Belgium
[2] Skolkovo Institute of Science and Technology, Skolkovo Innovation Center, Nobel St. 3, Moscow 143026, Russia

[a)] **Author to whom correspondence should be addressed:** vishank.iitk@hotmail.com
[b)] xavier.gonze@uclouvain.be

ABSTRACT

The diffusion of Li in bulk Si and crystalline LiSi is investigated over a wide range of temperatures employing first-principles calculations based on density functional theory, transition state theory, and the kinetic Monte Carlo method. Nuclear quantum effects are incorporated by computing the vibrational spectrum and its effect on the effective energy barrier. The Li diffusion coefficient in bulk Si calculated with such quantum effects is ~33% lower than the classical limit near room temperature due to higher effective energy barrier and tends to the classical limit at a high temperature (>1000 K). The presence of anharmonicity, estimated by the quasiharmonic approximation and the $cB\Omega$ model, increases the diffusion coefficient by ~60%. For Li diffusion in LiSi with multiple vacancy jumps, we obtain an effective diffusion barrier of 0.27 eV ± 0.01 eV. In the Li–Si system, the quantum mechanical effects are only marginally significant at room temperature.

I. INTRODUCTION

The use of silicon as an anode material in Li-ion batteries (LIB) has been investigated intensely for many years. With a gravimetric capacity about ten times higher than graphite, Si-based anodes can drastically improve the energy density of current LIBs. However, their actual use is limited by a huge volume change (up to 300%) during charging and discharging.[1] This is due to complex structural transformations that Si experiences during Li insertion and removal.[2] In order to understand the structural changes, it is paramount to investigate the kinetics of Li in both bulk Si and various lithiated phases.

Several experimental methods such as the potentiostatic and/or galvanostatic intermittent titration techniques (PITT and GITT),[3] nuclear magnetic resonance (NMR),[4] electrochemical strain mapping (ESM),[5] and electrochemical impedance spectroscopy (EIS)[6] have been used to estimate Li diffusion coefficients in Si-based anode materials. Nevertheless, an accurate quantitative measurement of the Li diffusion coefficient in lithiated Si is still a challenging task because of phase transformations upon lithiation, precise sample preparation, and controlling other experimental parameters. Consequently, there is a large discrepancy in the experimentally reported values of Li diffusivity in lithiated Li_xSi ($x \geq 1$), spanning 4 orders of magnitude from 10^{-8} cm^2/s to 10^{-12} cm^2/s in room temperature values.[3,5–8]

First-principles methods based on density functional theory (DFT) have been very successful in providing an atomic-level description of diffusion mechanisms as well as overall diffusivity values. Such DFT studies have shown that Li occupies the tetrahedral (T_d) site in the Si lattice during the initial phase of lithiation and jumps to the adjacent T_d site via the hexagonal (H_x) transition site.[9] The diffusion barrier calculated from first-principles (0.59 eV)[9–11] is in reasonable agreement with the experimental value of 0.655 eV ± 0.01 eV.[12] However, most of these first-principles studies have been limited to the calculation of the diffusion barrier, while the diffusion coefficient is, at most, estimated.

In order to study the kinetics, DFT based *ab initio* molecular dynamics (AIMD) simulations have been used frequently to compute the diffusion coefficient. Despite the overall success of such simulations, in particular, for electrolytes,[13] the technique is limited to fast diffusion processes. It is, indeed, computationally expensive and sometimes even infeasible to get the desired convergence,

especially in dilute doping limits. Consequently, the diffusion coefficients of Li in Li_xSi ($x \geq 1$) calculated from AIMD simulations at 300 K show a variation of 5 orders of magnitude spanning from 10^{-9} cm^2/s to 10^{-14} cm^2/s.[14–18] In order to speed up the simulation, often AIMD simulations are generally conducted at high temperatures to accelerate the diffusion process, and the diffusion coefficient is then extrapolated to room temperature. The discrepancy in the reported values can be due to small errors, which are then amplified by the extrapolation to room temperature. Additionally, the diffusion mechanism at a high temperature may be qualitatively different than at room temperature and the extrapolation of the diffusion coefficient might not be a plausible approximation, especially if there is a phase change and a consequent change in the diffusion mechanism. In principle, enhanced sampling methods such as metadynamics can also be used on top of AIMD simulations to speed up the process; however, finding a set of collective variables to describe the diffusion process can be challenging.[19]

Recently, Moon *et al.*[20] studied Li diffusion in Si and various Li_xSi alloys using the Kinetic Monte Carlo (KMC) method based on the energy barriers calculated from first principles. They found a diffusion coefficient of Li in LiSi in the range of 10^{-11} cm^2/s -10^{-12} cm^2/s at 300 K with an effective barrier of 0.306 eV. Although their results are in good agreement with the experimental data at 700 K, it is not clear whether they used classical or quantum approximations in calculating the diffusion prefactor for the KMC studies. Moreover, the treatment of atomic nuclei as pointlike classical particles may lead to inaccuracies in describing the motion of Li atoms, even though to a lesser extent as compared to protons.[21] A few studies[21–24] have shown that nuclear quantum effects have a significant contribution to the vibrational properties of lithium, which, in turn, affects the jump rate and the overall diffusion coefficient. This suggests that it is not trivial to neglect these effects *a priori* without any quantitative or qualitative assessment, which has not yet been done for the Li–Si system.

An approach to obtain a non-classical description of diffusion based on the transition state theory (TST) has been proposed.[24,25] The suggested method is computationally cheaper, yet it provides a comparable accuracy to an expensive path integral (PI) based on AIMD methods. This approach has been successfully tested for hydrogen diffusion in metals,[25] Li diffusion in graphite,[24] self-diffusion of Si,[26] and many more systems.[27–29] This method is often used with the harmonic approximation for computing the phonon frequencies, and it is important to estimate the effect of anharmonicity in the system that might become significant at a high temperature.

The literature on anharmonicity in diffusion discusses mainly two types of effects: (1) those due to the change in the lattice parameter owing to thermal expansion at a high temperature[30,31] and (2) those due to the phonon–phonon interactions.[32,33] The first effect, i.e., the volume change, is often studied through the quasiharmonic approximations (QHAs) that provide a first order anharmonic correction.[34] However, it can underestimate the phonon frequency change when the phonon–phonon interactions contribute significantly in phonon softening at high temperatures.[32] In order to address both effects, Varotsos and Alexopoulos proposed the $cB\Omega$ model[35–37] that connects the Gibbs free energy (for defect formation or for migration) to the isothermal bulk modulus (B) and the volume per atom (Ω), changing as a function of temperature. The model gives slightly better agreement with the experimental data as compared to a similar model proposed earlier by Wert and Zener that connects the Gibbs free energy of formation to the shear modulus, μ, of the material.[38,39]

In the present work, the methodology based on TST is followed and its limitations are discussed along with a measure of anharmonic effects in calculating the diffusion coefficient. We examine Li interstitial diffusion in bulk Si, as well as Li diffusion in the crystalline lithiated phase LiSi. The LiSi phase is selected as it is difficult to observe its formation in room temperature experiments due to the slow kinetics of formation and narrow temperature range of stability.[40,41] Thus, it is often not considered in studying the Li–Si system.[3,42] However, it is a stable phase below 600 K, and it can be synthesized at a pressure of 1 GPa–2.5 GPa and a temperature range of 773 K–993 K (500 °C–700 °C).[43,44] Thus, our study on Li diffusion in LiSi might reduce the gap in the literature of the LiSi alloy. The effect of anharmonicity is estimated by the $cB\Omega$ model and compared with the quasiharmonic approximation. For this purpose, we compute from first principles the temperature-dependent primitive cell volume and bulk modulus for the LiSi phase, which had not yet been computed or measured, to the best of our knowledge. Our results provide a consistent interpretation of the experimental data and an analysis of the quantum mechanical and anharmonic effects for Li diffusion in the Li–Si system.

The paper is structured as follows: Sec. II presents the theoretical details of the extended TST formalism to obtain the diffusion coefficient and the computational details used for calculations. Section III provides the results obtained for Li diffusion in bulk Si. Section IV provides those for Li diffusion in the c-LiSi phase, and finally, Sec. V summarizes our major findings and presents our concluding remarks.

II. METHODS

A. Theoretical approach

The diffusion coefficient of a single interstitial atom in bulk solid can be obtained by the transition state theory. Following Vineyard's work,[45] it is written as

$$D_{TST}(T) = \frac{1}{6} z R^2 \tau(T), \tag{1}$$

where z is the number of equivalent jumps, R is the jump distance, and τ is the jump rate that depends on the temperature T. The jump rate is, in turn, expressed in terms of the vibrational free energy difference, ΔF^{vib}, and the diffusion energy barrier, ΔE, between the initial and the saddle point as[45]

$$\tau(T) = \frac{kT}{h} e^{-[\Delta E + \Delta F^{vib}(T)]/kT}. \tag{2}$$

If we consider the harmonic approximation for the lattice vibrations with a quantum mechanical expression, ΔF_Q^{vib} can be written in terms of the vibrational frequencies at the saddle point (S) and at the initial point (0) as

$$\Delta F_Q^{vib}(T) = \sum_i^{N-1} \left\{ \frac{1}{2} h\nu_i^S + kT \ln\left[1 - e^{-h\nu_i^S/kT}\right] \right\} - \sum_i^{N} \left\{ \frac{1}{2} h\nu_i^0 + kT \ln\left[1 - e^{-h\nu_i^0/kT}\right] \right\}. \tag{3}$$

The classical limit of this expression is given by[24]

$$\Delta F_C^{vib}(T) = kT\left\{\sum_i^{N-1} \ln\left(\frac{h\nu_i^S}{kT}\right) - \sum_i^{N} \ln\left(\frac{h\nu_i^0}{kT}\right)\right\}, \tag{4}$$

where ν_i is the vibrational frequency of the ith mode with $h\nu_i$ being the quantum of energy of the harmonic oscillator. The superscripts S and 0 denote the initial point and the saddle point, respectively, while the subscripts Q and C represent the quantum and classical expressions, respectively. The summation in the saddle point case runs only until $N-1$ because there is one degree of freedom less corresponding to the imaginary frequency associated with the negative curvature at the saddle point.[46] The complete derivation of the free energy using the partition function with the harmonic approximation is explained in Appendix A. Substituting the expression for ΔF^{vib} from Eq. (3) in Eq. (1), the diffusion coefficient can be written as

$$D_Q(T) = \frac{1}{6} zR^2 \frac{kT}{h} \frac{\prod_i^N 2\sinh\left(\frac{h\nu_i^0}{2kT}\right)}{\prod_i^{N-1} 2\sinh\left(\frac{h\nu_i^S}{2kT}\right)} e^{-\Delta E/kT}. \tag{5}$$

This expression for the diffusion coefficient correctly approaches the classical limit given by the TST at high and low temperatures,[25,45]

$$\lim_{T\to\infty} D_Q(T) = D_C(T) = D_{\mathrm{TST}}(T) = \frac{1}{6} zR^2 \frac{\prod_{i=1}^N \nu_i^0}{\prod_{i=1}^{N-1} \nu_i^S} e^{-\Delta E/kT}, \tag{6}$$

$$\lim_{T\to 0} D_Q(T) = D_{\mathrm{TST}+\Delta\mathrm{ZPE}}(T) = \frac{1}{6} zR^2 \frac{kT}{h} e^{-(\Delta E+\Delta\mathrm{ZPE})/kT}, \tag{7}$$

where ZPE is the zero-point energy, defined as the low temperature limit of Eq. (3) so that

$$\Delta ZPE = \lim_{T\to 0} \Delta F_Q^{vib}(T) = \sum_{i=1}^{N-1} \frac{h\nu_i^S}{2} - \sum_{i=1}^{N} \frac{h\nu_i^0}{2}. \tag{8}$$

The diffusion equation taking into account the quantum approximation [Eq. (5)] can also be written in the Arrhenius form as[25]

$$D_Q(T) = D_{QA}^*(T) e^{-\Delta E_{QA}(T)/kT}, \tag{9}$$

where the temperature-dependent pre-factor and the energy barrier are given by

$$D_{QA}^*(T) = \frac{1}{6} zR^2 \frac{kT}{h} \times \frac{\prod_i^N \sinh\left(\frac{h\nu_i^0}{2kT}\right) \exp\left[\sum_{i=1}^{N-1} \frac{h\nu_i^S}{2kT} \coth\left(\frac{h\nu_i^S}{2kT}\right)\right]}{\prod_i^{N-1} \sinh\left(\frac{h\nu_i^S}{2kT}\right) \exp\left[\sum_{i=1}^{N} \frac{h\nu_i^0}{2kT} \coth\left(\frac{h\nu_i^0}{2kT}\right)\right]}, \tag{10}$$

$$\Delta E_{QA}(T) = \Delta E - kT \sum_{i=1}^{N} \frac{h\nu_i^0}{2kT} \coth\left(\frac{h\nu_i^0}{2kT}\right) + kT \sum_{i=1}^{N-1} \frac{h\nu_i^S}{2kT} \coth\left(\frac{h\nu_i^S}{2kT}\right). \tag{11}$$

The above equations present the correct high and low temperature limits such that Eq. (9) approaches Eqs. (6) and (7), respectively. Note that Eqs. (10) and (11) are corrected versions of Eqs. (9) and (10) of Ref. 25. Although Eq. (9) includes the zero-point energy, it does not take into account the quantum tunneling effects that might play a significant role for small Li atoms. Fermann and Auerbach[47] suggested an approach to include the quantum tunneling effects as a correction factor Γ to provide the overall diffusion equation as

$$D_{Q+\Gamma} = D_Q \Gamma, \tag{12}$$

where Γ is a dimensionless multiplying factor incorporating the effect of thermally activated incoherent tunneling to the diffusion equation. The factor Γ is defined as[47]

$$\Gamma(T) = \frac{e^{\Delta E/kT}}{1 + e^{2\pi\Delta E/h|\nu^\ddagger|}} + \frac{1}{2} \int_{-\infty}^{\pi\Delta E/h|\nu^\ddagger|} e^{h|\nu^\ddagger|\theta/\pi kT} \mathrm{sech}^2\theta d\theta, \tag{13}$$

in which $\nu^\ddagger$ is the imaginary frequency associated with the curvature at the saddle point. The above expression for Γ must be evaluated by using numerical integration with a sufficiently lower limit for $-\infty$. At a low temperature, Γ becomes proportional to $e^{\Delta E/kT}$,[47]

$$\lim_{T\to 0} \Gamma(T) \to e^{\Delta E/kT} e^{-2\pi\Delta E/h|\nu^\ddagger|} \left(1 + \frac{2\pi kT}{h|\nu^\ddagger|}\right), \tag{14}$$

thus canceling the temperature dependence term $e^{-\Delta E/kT}$, resulting in a non-zero diffusion coefficient as known from both theoretical and experimental results. However, at a high temperature, it becomes[47]

$$\Gamma(T) = 1 + \sum_{n=1}^{\infty} \frac{1}{n!} \left(\frac{h|\nu^\ddagger|/kT}{\pi}\right) \left[\frac{\theta_0^n}{1 + e^{2\theta_0}} + \frac{1}{2} \int_{-\infty}^{\theta_0} \theta^n \mathrm{sech}^2\theta d\theta\right], \tag{15}$$

where $\theta_0 = \pi\Delta E/h|\nu^\ddagger|$. This expression tends to 1 as T increases; thus, the diffusion coefficient converges to the classical diffusion equation [Eq. (6)]. Therefore, this quantum tunneling correction shows the correct high and low temperature limits. As all the ingredients required for calculating Γ (ΔE and ν_i) are already available in evaluating Eq. (5), we used this approach to include the quantum tunneling correction. It should be noted that in the original study,[47] the correction factor Γ was multiplied by the diffusion coefficient obtained by the classical TST approach, while in the present work, the expression based on the quantum-mechanical approximation, according to Eq. (9), is used.

The anharmonic effects due to the volume expansion can be studied consistently using the quasiharmonic approximation. In this approach, the diffusion barrier varies as a function of volume V, at a given temperature T, i.e., $\Delta E(T) = \Delta E(V(T))$, where $V(T)$ is determined by minimizing the free energy curve vs volume for a given T using the QHA.[48–50]

In the QHA, all the phonon frequency shifts are associated with the volume change so that phonon frequencies are explicitly volume dependent and are temperature dependent only through the thermal expansion. Although this approach is a common practice in the literature to incorporate anharmonic effects, it does not include the anharmonic effects caused by phonon–phonon interactions or in other words explicit temperature dependence. The $cB\Omega$ model

proposed by Varotsos and Alexopoulos[35,51] incorporates both the volume and phonon–phonon temperature dependence, approximately, by defining the diffusion energy barrier as

$$\Delta E(T) = cB(T)\Omega(T), \tag{16}$$

where $B(T)$ is the isothermal bulk modulus, $\Omega(T)$ is the mean volume per unit atom, and c is the dimensionless constant with respect to temperature and pressure. The constant c can be obtained by fitting Eq. (16) with the diffusion energy barrier (ΔE) estimated from the experimental data or with the one calculated from first principles at $T = 0$.

Despite the accuracy of the abovementioned approach to study diffusion, as it is based on TST, it shares similar challenges. One of the main restrictions is that the initial and the final point configuration need to be known *a priori* to find the saddle point of the jump, which can be difficult in some cases, especially in amorphous systems.[10] However, in most of the crystalline systems, one can identify stable sites for the diffusing species from ground-state calculations. Jumps between these sites can then be studied by nudged-elastic band (NEB)[52] or climbing-image nudged-elastic band (CI-NEB)[53] methods, providing the saddle point configuration. Thus, it is in fact a limitation of the NEB method.

The second limitation that arises from the use of TST is that it gives the diffusion coefficient based on only one type of jump, which might not be the case in most diffusion studies.[20,54,55] However, one can use methods such as KMC simulations[56,57] to get the effective diffusion coefficient from multiple jumps.[20,54] The KMC method treats each jump as an independent process, I, with a jump rate τ_i defined as[45,58]

$$\tau_i = \gamma_i e^{-\Delta E_i/kT}, \tag{17}$$

where γ_i is the attempt frequency, ΔE_i is the energy barrier obtained by a NEB calculation, k is the Boltzmann constant, and T is the temperature. Substituting Eqs. (5) and (6) in Eq. (1), the jump rate (τ_i) can be obtained with the quantum and classical approximations, respectively. The detailed KMC algorithm for simulating the time evolution can be found in the literature,[59–61] and the main steps are mentioned in Appendix B. It should be noted that the effective diffusion coefficient thus obtained are discrete data points for a particular temperature T, unlike the continuous curve obtained by TST. The overall diffusion equation can then be obtained by fitting these data points.

The effect of using a quantum mechanical approximation and anharmonicity on the diffusion coefficient is the center of our study. Since lithium is a relatively light atom, a large zero-point energy is present for the vibrations in which it has a large participation ratio, thus potentially impacting the diffusion constant. An assessment on the validation of the harmonic approximation and quantum tunneling corrections will provide a useful insight on the Li diffusion in bulk Si and c-LiSi.

B. Computational details

The first-principles total energy calculations were performed with DFT as implemented in the ABINIT code[62–65] using a plane-wave basis set within the generalized-gradient approximation (GGA-PBE).[66] The converged plane-wave cutoff energy was 32 Ha (~871 eV) and 12 Ha (~327 eV) for bulk Li and Si, respectively. For bulk Si doped with Li and for LiSi structure, a cutoff energy of 32 Ha (~870.76 eV) was used. ONCVPSP pseudopotentials[67,68] were used with 1*s* and 2*s* electrons as valence electrons for Li, while for Si, 3*s* and 3*p* electrons were treated as valence electrons.

A supercell of 96 Si atoms (2 × 3 × 2 of the conventional unit cell) was used for studying bulk Si and then was added with one interstitial Li atom, and a supercell of 128 atoms (2 × 2 × 2 of the primitive unit cell) was considered for the c-LiSi structure and then was depleted of one Li atom. For sampling the Brillouin zone, a 2 × 2 × 2 Monkhorst–Pack k-point mesh was used. The kinetic energy cutoff and the k-point sampling were obtained from convergence studies with a tolerance level of 0.5 mHa/atom (~14 meV/atom). The self-consistent field (SCF) cycles for the total energy calculations were converged until the difference in forces between the two consecutive cycles was less than 10^{-7} Ha/Bohr (0.005 meV/Å) twice in a row. The structural relaxations were performed using the Broyden–Fletcher–Goldfarb–Shanno (BFGS) minimization until the forces on each atom were smaller than 5 × 10^{-6} Ha/Bohr (0.3 meV/Å). For metallic systems, a Gaussian smearing of 0.01 Ha (0.23 eV) was used for the occupation of states.[69]

In the case of Li diffusion in bulk Si, the most stable position for a single Li atom is the tetrahedral (T_d) interstitial site. Li atoms diffuse by jumping to the next vacant T_d site via an hexagonal (H_x) site.[9,70] The corresponding jump distance, i.e., the distance between two T_d sites in a diamond lattice, is $a\sqrt{3}/4$. The energy barrier for Li diffusion was calculated by the NEB method.[53] In order to find the diffusion barrier profile, at least 7 images were used with 2 fixed (initial and final images) and 5 dynamic images. All the images were relaxed until the absolute energy difference was less than 10^{-5} Ha (0.27 meV). The effective diffusion coefficient of Li in LiSi was obtained through KMC simulations. In order to obtain better statistics, each KMC simulation was run for 10 000 steps and averaged over 40 000 sites, an approach suggested in previous KMC studies.[54,61]

The TST formalism requires to compute the phonon frequencies only at the Γ point. This is what was done in calculating the diffusion coefficient for computational efficiency. However, the full phonon band structures of smaller cells were also produced for illustration purposes. All these calculations were performed using the density functional perturbation theory (DFPT) as implemented in the ABINIT code.[71–73]

For computing the volume expansion using the QHA, the phonon contribution of the free energy has been calculated at three volumes, i.e., at the equilibrium point as well as for 1% and 6% volume expansion at temperatures from 10 K to 1000 K with a step of 10 K, and fitted with a quadratic expression for each temperature. The total energy was calculated at 34 points starting from a structure with 3% lower volume to the one with 30% higher volume than the equilibrium structure and fitted with a 4th order polynomial, appropriate in that range. The summation of the total energy and the phonon free energy gives the free energy curves at a temperature interval of 10 K. The equilibrium volume is thus obtained by minimizing the free energy curves, and the isothermal bulk modulus, $B(T)$, is obtained as[74]

$$B(T) = \left.\frac{\partial^2 F}{\partial V^2}\right|_{V(T)} V(T). \tag{18}$$

The volume-dependent diffusion barrier in the QHA was obtained by computing first the energy barrier calculated at 0 K and at an increased volume corresponding to high temperature (T_h), say 1000 K, and then performing a linear interpolation of the volume-dependent energy between these two values,

$$\Delta E(T) = \Delta E_0 + \frac{\Delta E_{T_h} - \Delta E_0}{V_{T_h} - V_0}(V(T) - V_0), \tag{19}$$

where ΔE_0 and V_0 are the diffusion barrier and mean volume per atom calculated at 0 K from first principles, respectively; ΔE_{T_h} and V_{T_h} represent the diffusion barrier and the associated mean volume per unit atom calculated at a high temperature T_h, respectively; and $V(T)$ represents the mean volume per unit atom at a given temperature T. In the case of bulk Si, the data from Ref. 50 have been used to calculate $V(T)$ and $B(T)$, while for LiSi, these thermodynamic quantities have been calculated from DFPT as implemented in ABINIT[71,72] with the abovementioned computational parameters.

III. Li DIFFUSION IN BULK Si

A. Li insertion into bulk Si

In bulk Si, the most stable position for a single Li atom is the tetrahedral (T_d) interstitial site.[9] The optimized lattice parameters for our pristine 96-atom Si supercell are 10.93 Å, 10.93 Å, and 16.41 Å, which increase to 10.94 Å, 10.94 Å, and 16.41 Å after the addition of 1 interstitial Li atom. It is less than 0.1% increase in the lattice parameters. Figure 1 shows the effect of one Li atom addition on the electronic density of states (DOS) of bulk Si (16-atom supercell, for illustration purposes) in an energy window corresponding to the valence and conduction states spanning the interval [−15 eV, 5 eV] around the Fermi energy. Upon Li addition, the DOS is almost unchanged. However, the peak heights near the conduction bands are modified since the 2s electron of the interstitial Li is added to the conduction band. Consequently, the Fermi energy moves into the conduction band, making it a metallic system. The Fermi energy increases by 0.34 eV upon addition of one Li atom to the 16-atom supercell.

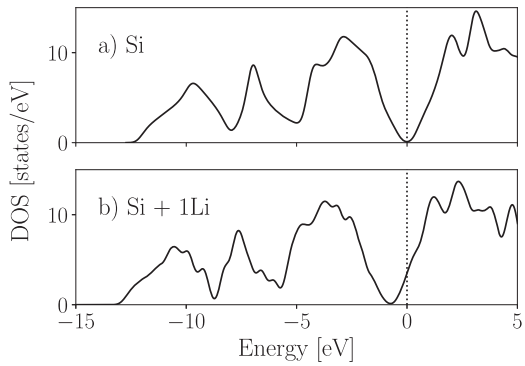

FIG. 1. Electronic density of states of (a) bulk Si and (b) bulk Si with 1 Li atom at the T_d interstitial site. The Fermi energy is set to zero on the *x*-axis (dotted line). A 2 × 2 × 2 supercell with 16 Si atoms has been used to simulate bulk Si. These small-cell results are shown for illustration purpose only.

Figure 2 shows the effect of Li addition on the vibrational properties of bulk Si (16-atom cell, for illustration purpose). First of all, after Li addition, three new high-energy vibrational modes are observed. These three modes represent the vibrational frequency of the light Li atom in the three spatial dimensions. In order to check the convergence with respect to the supercell size, supercells of 54 atoms (3 × 3 × 3 of the primitive unit cell) and 96 Si atoms (2 × 3 × 2 of the conventional unit cell) were also considered. The corresponding diffusion barriers and diffusion coefficients are included in the supplementary material (see Fig. S1). Convergence tests confirmed that a supercell of 96 Si atoms is large enough to avoid any inter-atomic interaction across periodic boundaries, and thus, the 96-atom supercell was used to study bulk and doped Si.

The partial phonon density of states (PPDOS) from this 96-atom supercell (Fig. 3) allows us to identify the three modes predominantly associated with localized vibrations of the interstitial Li atom in the three Cartesian directions. Moreover, these modes also involve significant Si displacements, i.e., the interstitial Li atom cannot vibrate freely without affecting the neighboring Si atoms. Despite this collective behavior, we shall call such modes "Li modes" in this work. These coupled vibrations are due to the partial charge transfer between the interstitial Li and the neighboring Si atoms that inhibit the free movement of the Li atom like a neutral interstitial atom.[9] Thus, unlike in the case of hydrogen diffusion in metals (metals are heavier),[25] here, it is not possible to assume that

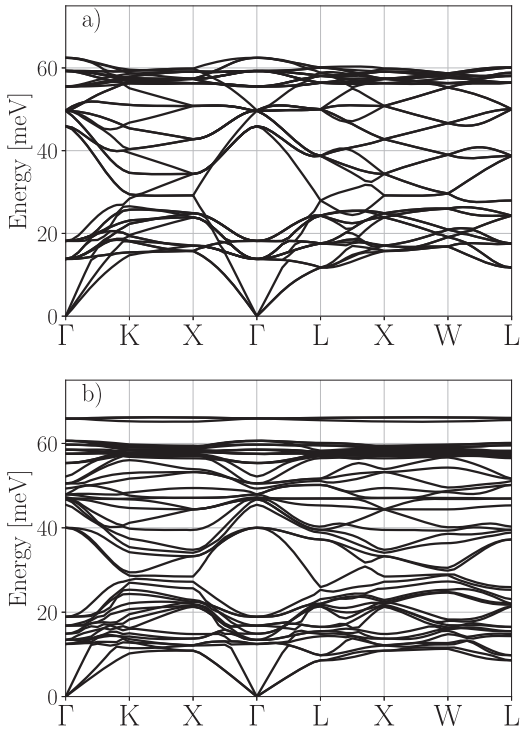

FIG. 2. Phonon band structures of (a) bulk Si and (b) bulk Si with 1 Li atom at the T_d interstitial site. The three extra Li modes are clearly seen around 65 meV in the latter. A 2 × 2 × 2 supercell with 16 Si atoms has been used to simulate bulk Si. These small-cell results are shown for illustration purpose only.

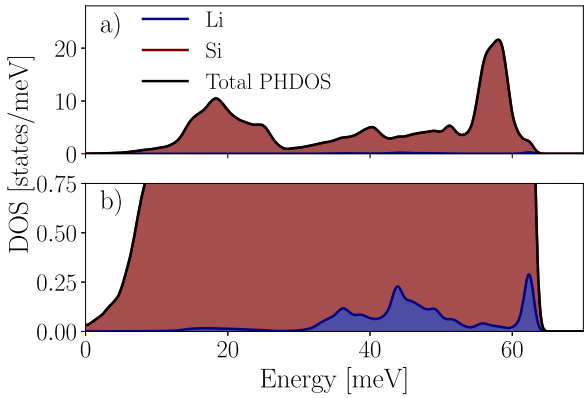

FIG. 3. (a) Partial phonon density of states (PPDOS) of a 96-atom supercell with 1 Li atom and (b) a zoomed-in image of the same PPDOS showing the three peaks corresponding to the Li atom overlapping with those of Si atoms.

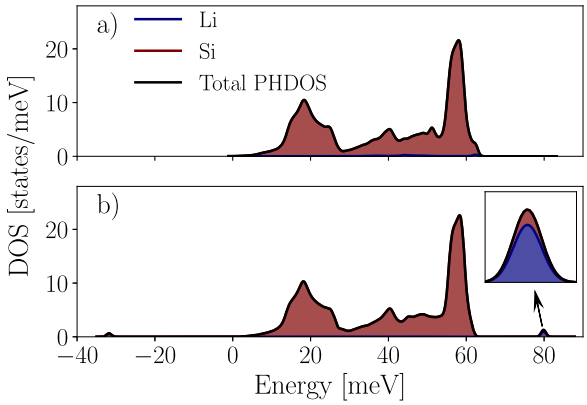

FIG. 5. Partial phonon density of states (PPDOS) of bulk Si (96 atoms) with one Li (a) at the T_d site (minimum energy geometry) and (b) at the H_x site (saddle point geometry). At the saddle point, two Li modes become degenerate at a higher vibrational frequency (at 80 meV) and the third one shifts to an imaginary frequency (at −32 meV) represented as negative for illustrating purposes, corresponding to the vibration in the direction of propagation at the saddle point.

the light Li atoms move freely in the host lattice. Therefore, all the phonon modes have to be considered for calculating the diffusion coefficient. After analyzing the effect of Li insertion into bulk Si, in Sec. III B, the diffusion of this interstitial Li atom in bulk Si is discussed.

B. Diffusion mechanism: Interstitial diffusion

The energetically favorable diffusion pathway for a single Li atom is $T_d \rightarrow H_x \rightarrow T_d$ as suggested by previous studies.[9] The diffusion barrier computed by the NEB method is 0.59 eV (Fig. 4), which is in good agreement with previous experimental and theoretical studies.[9,12,75] As expected, the diffusion path is symmetric across the barrier.

Figures 5(a) and 5(b) show the phonon density of states for the initial (Li at T_d site) and saddle (Li at H_x site) point configurations, respectively. The initial point configuration shows three Li modes coupled with Si, as mentioned in Sec. III A. For the saddle point configuration, two of these Li modes become degenerate at 80 meV and the remaining one is an unstable mode with an imaginary frequency of 32 meV [represented as negative in Fig. 5 (b)]. The degeneracy of the two high-energy Li modes comes from the crystal symmetry, and the unstable mode comes from the displacement in the direction that connects the two local minima. However, similar to the initial state, all three Li modes are still coupled with Si. The hardening of the doubly degenerate mode can be understood from the proximity of the Li atom to Si atoms at the saddle point, causing faster increase in the potential felt by the Li atom when vibrating perpendicular to the transition path direction.

Figure 6 shows the difference in vibrational free energy ΔF_C^{vib} and ΔF_Q^{vib} calculated adopting the classical and quantum approximations as per Eqs. (4) and (3). At 0 K, the quantum ΔF_Q^{vib} has a finite value of 16 meV, while the classical approximation reaches zero. The difference between both approximations reduces to ~7 meV

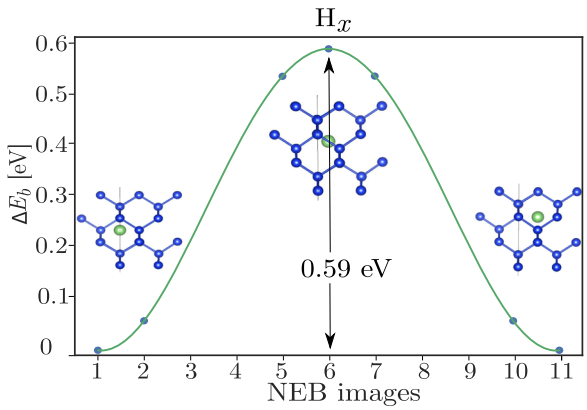

FIG. 4. Diffusion barrier calculated by the NEB method for one Li atom diffusing in bulk Si.

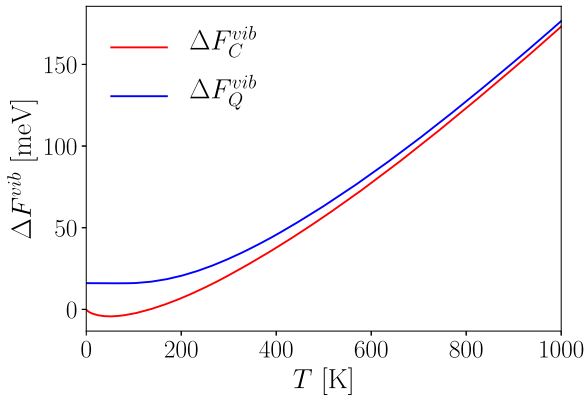

FIG. 6. Temperature dependence of the change in vibrational free energy between the initial and the saddle point with classical (red) and quantum (blue) approximations.

at room temperature as they converge to the same value at a high temperature.

These vibrational energies were used to calculate the diffusion coefficient according to Eqs. (6) and (5) using the classical and quantum approximations, respectively. The jump distance is the distance between two tetrahedral voids in a diamond lattice, i.e., 2.368 Å. The calculated diffusion coefficient is shown on a logarithmic scale vs $1000/T$ (Fig. 7), showing an Arrhenius-like behavior for both the quantum (blue) and classical (red) theories. Their ratio is also shown in Fig. 8: it is close to one at a high temperature (>1000 K), while it can be significantly smaller at a lower temperature, e.g., 0.6 near room temperature. Both approaches are in reasonable agreement with the experimental data of Pell[12] and the theoretical calculation of Fedorov *et al.*,[76] especially at high temperatures, given the usual uncertainties and rapid changes with temperature of such quantities. The pre-factor of 1×10^{-3} cm^2/s calculated for Li diffusion in bulk Si is in reasonable agreement with the experimental value of 2.3×10^{-3} cm^2/s $\pm$ 0.2×10^{-3} cm^2/s. However, the other values reported in the literature (Refs. 5, 8, and 18) at room temperature are at least 3–4 orders of magnitude higher.

Johari *et al.*[18] studied Li diffusion by the means of AIMD during the mixing of Li and Si atoms, where the host lattice transforms from the c/a-Si in the beginning to the a-Li$_x$Si phase. We know that Li diffuses at least one order of magnitude faster in Li$_x$Si phases as compared to bulk Si,[3] which justifies a higher value. Balke *et al.* used a value of ~10^{-8} cm^2/s–10^{-10} cm^2/s to study the diffusion of Li-ions by means of ESM in a-Si, where Li diffusivity is expected to be higher as compared to c-Si.[18,76] Moreover, it was not a direct measurement of Li diffusivity, and they also reported some problems during probing the sample, which they suggested was either due to a higher or lower Li-ion mobility than they assumed. The result of Yoshimura *et al.*[8] (2×10^{-11} cm^2/s) is the closest, among these three, to the experimental data of Pell.[12] They studied Li diffusion in a single crystal Si by using bipolar cells; however, they were not sure if it was without any alloy formation of Li$_x$Si during polarization, which explains why their reported diffusivity value is higher.

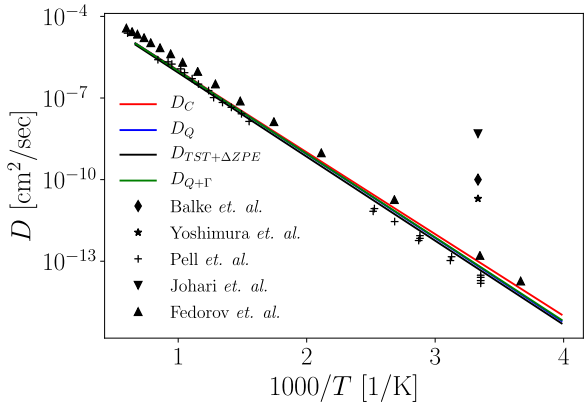

FIG. 7. Temperature dependence of the diffusion coefficient calculated for Li in bulk Si. Blue and red lines represent the diffusion coefficient calculated with quantum and classical approximations, respectively. The black line shows the classical approximation with *ZPE* correction only, and the green line represents the quantum approximation with quantum tunneling correction. The markers represent the values reported in Refs. 5, 8, 18, 76, and 77.

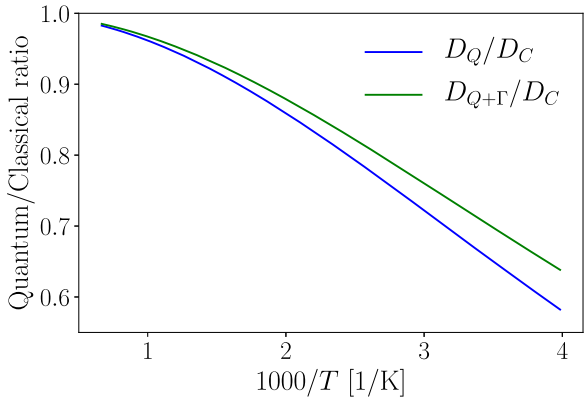

FIG. 8. Temperature dependence of the effect of quantum corrections on the diffusion coefficient measured as a ratio of D_Q/D_C (blue). The ratio $D_{Q+\Gamma}/D_C$ (green) shows the added effect of quantum tunneling corrections that slightly increases the diffusion coefficient in the low temperature regime.

C. Effect of quantum mechanical approximation

The diffusion equation in the Arrhenius form with the quantum mechanical approximation has a temperature-dependent energy barrier (ΔE^*_{QA}) instead of a constant energy barrier with the classical approximation. Figure 9(a) shows this temperature dependence of the energy barrier along with the constant barrier from the classical TST framework. The effective activation barrier increases in the lower temperature range to reach a maximum and then decreases, tending to converge to the classical limit at a high temperature. At 0 K, the effective energy barrier is higher than the classical limit because of the zero-point energy (ΔZPE).

Similarly, the effective diffusion pre-factor (D^*_{QA}) increases in the low-temperature regime to reach a maximum and then decreases to tend to the classical limit in the high-temperature regime [Fig. 9(b)]. However, it is worth noting that due to a significant contribution from quantum tunneling effects (Γ) in the low-temperature range (Fig. 10), the corrected diffusion pre-factor ($D^*_{QA}.\Gamma$) does not reach a maxima but rather diverges at a low temperature. This exponentially increasing value of ($D^*_{QA}.\Gamma$) cancels out the Arrhenius exponential temperature dependence in Eq. (9), thus resulting in a finite value of the diffusion coefficient in the low-temperature range.[47] The inclusion of quantum tunneling corrections slightly increases the diffusion coefficient ratio from 0.6 to 0.66 (Fig. 8), owing to an additional diffusion pathway. The effect is very small as tunneling effects are more prominent in the low temperature range. At a high temperature, Γ converges to 1 as expected since the quantum tunneling corrections become less important and the classical barrier jump is the dominating mechanism governing the overall diffusion coefficient.

The quantum mechanical approximation for the diffusion coefficient converges to the classical limit at a high temperature. It differs significantly from it only at a low temperature. The effects observed in the Li–Si system are the same as for the H-metal system and,

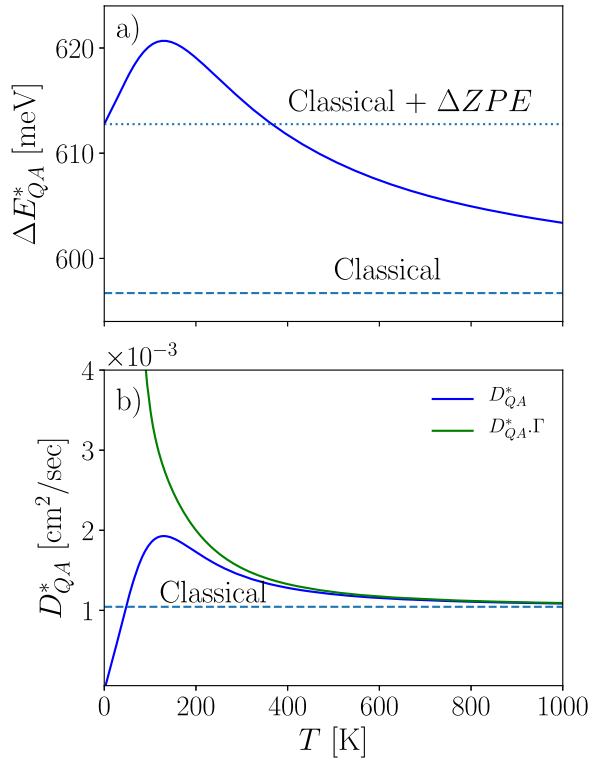

FIG. 9. Temperature dependence of (a) the effective activation barrier (ΔE_{QA}) and (b) the effective diffusion prefactor (D^*_{QA}), in blue, along with the quantum tunneling corrected prefactor ($D^*_{QA}.\Gamma$), in green. These parameters of the Arrhenius-like diffusion equation tend to their temperature-invariant classical limits, ΔE_m and D_0, respectively (dashed line), at high temperatures.

however, lower in magnitude. Thus, in order to clarify whether this suppression is due to the larger mass of Li or to the difference in the chemistry of Li–Si, we have performed a mass rescaling analysis in Sec. III D.

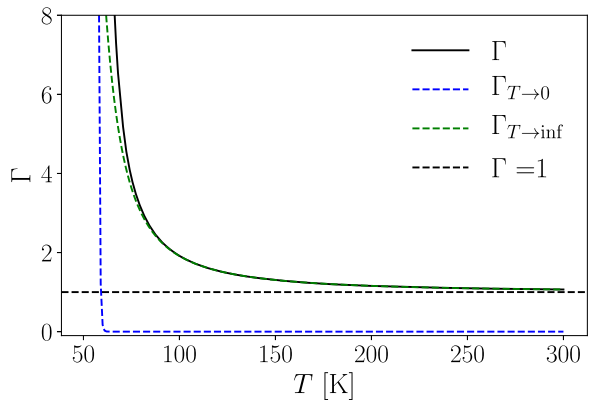

FIG. 10. Temperature dependence of the tunneling correction factor (Γ) for Li diffusion in bulk Si. Green and blue dashed curves are high- and low-temperature limits, respectively. At a high temperature, Γ converges to 1, represented by the black dashed line.

D. Effect of mass rescaling

In this mass rescaling analysis, the quantum mechanical effects on the diffusion coefficient were compared with the ones obtained if the lithium mass is replaced by the hydrogen mass, for which quantum effects are clearly seen even at room temperature in their diffusion in metals.

Due to such mass rescaling, there is a significant increase in the phonon frequencies of the vibrations that have a high participation ratio of the light atom (Li with H mass): the mass ratio being about seven, the vibration frequency ratio is approximately $\sqrt{7}$ for Li-dominated modes. The quantum modification of the vibrational free energy is much more pronounced, as shown in Fig. 11. At 0 K, the classical limit is absolutely zero, so the mass rescaling has no effect. For the quantum approximation, the zero-point energy slightly increases due to the scaling of frequencies and tends to the classical limit at a high temperature. At a high temperature, both approaches show lower values of the free energy difference due to the mass rescaling. After the mass rescaling, there is a significant quantum effect not only at room temperature but even at a high temperature (near 1000 K).

The classical (and quantum) decrease in the free energy with mass rescaling is a consequence of the higher vibrational frequency of the mode along the transition path in the initial geometry. The contribution from this mode is only present in the last term of Eqs. (4) and (3), i.e., in the initial point configuration. This extra mode is stretched to higher energy by the frequency ratio, resulting in a higher vibrational free energy difference (ΔF^{vib}) between the initial point and the saddle point configurations. Since all three Li modes overlap with the Si modes [see Fig. 3(b)], the latter are also affected by the mass rescaling, especially the two lateral high-frequency modes shown in Fig. 2(b), which are higher at the saddle point geometry than at the initial point geometry. The global qualitative picture of the mass rescaling effect at a high temperature is nevertheless dominated by the removal of the phonon mode rescaled in the saddle point configuration as compared to the initial point configuration.

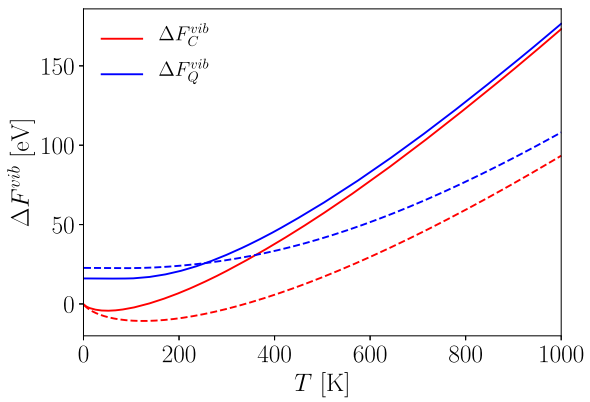

FIG. 11. Temperature dependence of the change in vibrational free energy with classical (red) and quantum (blue) approximations, when the Li mass is replaced by the H mass (rescaling), in view of separating the mass effect from the quantum/classical effect. Solid lines show the results obtained with the unchanged mass of the Li atom, and dashed lines show results with the rescaled mass of the Li atom.

This increase in the phonon frequencies due to mass rescaling shifts the diffusion coefficient upward, as shown in Fig. 12. However, in the low temperature range, it is shifted downward for the quantum case (D_Q) due to higher ΔF^{vib} after mass rescaling. Similar to what was obtained before mass rescaling, the quantum value after mass rescaling D_Q^r is lower than its classical counterpart D_C^r near room temperature, but it increases at a lower temperature as the quantum tunneling correction becomes dominant and eventually tends to flatten out surpassing D_C^r. Fermann and Auerbach[47] defined this temperature as the tunneling crossover temperature (T_x) below which the quantum tunneling is dominant. According to their definition, it is the temperature where the two linear sections could hypothetically intersect, which in the present case is ~150 K. This tunneling crossover temperature is roughly three times larger than the one before mass rescaling (~50 K).

Figure 13 shows the difference between the two approaches (classical and quantum), which is obviously much more pronounced near room temperature (and at a lower temperature) after mass rescaling. The ratio between the quantum and classical approximations at room temperature increases from ~30% to around 50% and 66% with ($D_{Q+\Gamma}/D_C$) and without (D_Q/D_C) tunneling correction, respectively (see the inset of Fig. 13). The inflection point in the $D_{Q+\Gamma}/D_C$ ratio curve represents the temperature above which tunneling corrections start becoming significant, resulting in a comparative increase in the diffusion coefficient with further lowering of temperature and eventually surpassing D_C above T_x. Moreover, the D_Q/D_C ratio shows that without this tunneling correction, the diffusion coefficient tends to 0 faster than its classical counterpart, which contradicts theoretical and experimental results.[47]

In order to disentangle the effect of the quantum tunneling correction, the ratio of $D_{Q+\Gamma}/D_Q$ is shown as a function of the inverse of temperature along with the mass-rescaled one (dashed line in Fig. 14). After the mass rescaling, the effect of quantum tunneling

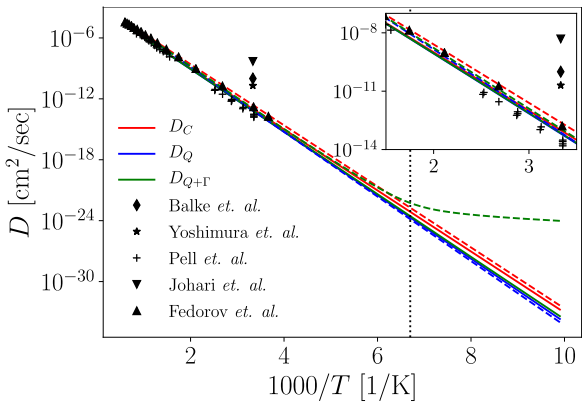

FIG. 12. Temperature dependence of the diffusion coefficient calculated using classical (red) and quantum (blue) approximations with quantum tunneling correction (green). Mass-rescaled values (see text) are represented by dashed lines. The corresponding room temperature values are shown in the inset. The dotted line marks the tunneling crossover temperature, T_x, for the mass-rescaled case. Markers represent the values reported in Refs. 5, 8, 18, 76, and 77. This crossover temperature is much lower when the mass is not rescaled and out of the temperature range shown here.

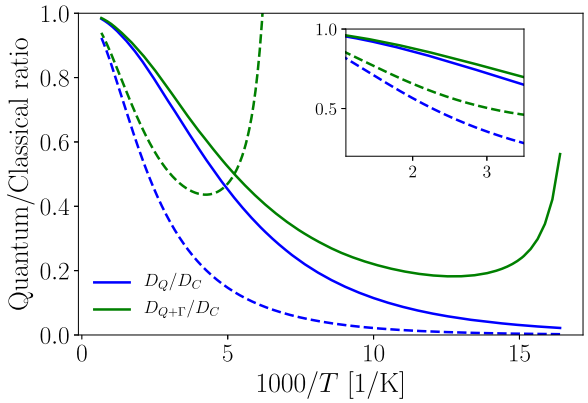

FIG. 13. Effect of mass rescaling on quantum corrections with respect to their classical counterparts is shown as a ratio, as a function of the inverse of the temperature (1000/T). Dashed lines represent the mass-rescaled values. Corresponding plots near room temperature are also shown in the inset.

corrections increases significantly: it reaches ~50% even near room temperature, while it was less than ~7% before mass rescaling. This analysis of mass rescaling shed light on how the heavier atomic mass of Li reduces quantum effects. However, the local chemical environment might also play an important role, complementing the understanding brought by the effective activation barrier and the effective diffusion pre-factor analysis in Fig. 8. Note that the current approach is based on the harmonic approximation, and to go one step beyond, Sec. III E discusses the effect of anharmonicity on the diffusion coefficient.

E. Effect of anharmonicity

Figure 15 compares the temperature dependence of the diffusion barrier ΔE calculated by the $cB\Omega$ model and the QHA along with the values obtained by NEB calculations at two different volumes. The diffusion barrier decreased by ~35 meV at higher volume

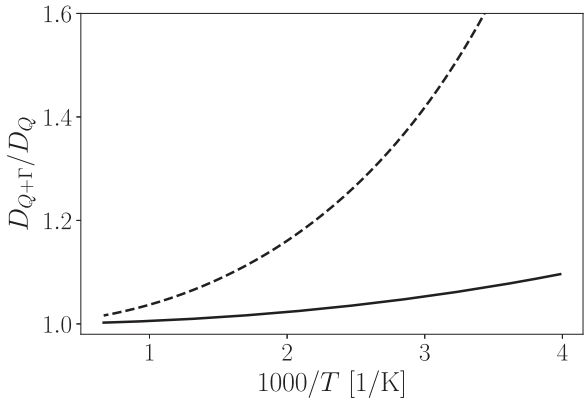

FIG. 14. Effect of including quantum tunneling corrections on the diffusion coefficient as measured by the ratio $D_{Q+\Gamma}/D_Q$, as a function of the inverse of the temperature (1000/T). Dashed lines represent the corresponding ratio after mass-rescaling.

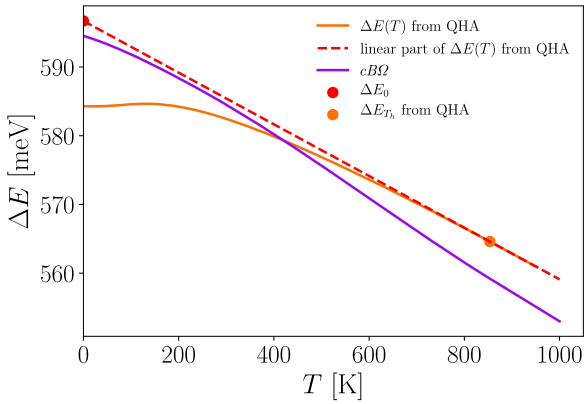

FIG. 15. Temperature dependence of the diffusion barrier obtained from the $cB\Omega$ model (purple curve) and the QHA (orange curve). Filled circles mark the values calculated using NEB calculations, and the dotted line shows the linear interpolation of the high temperature limit of the QHA.

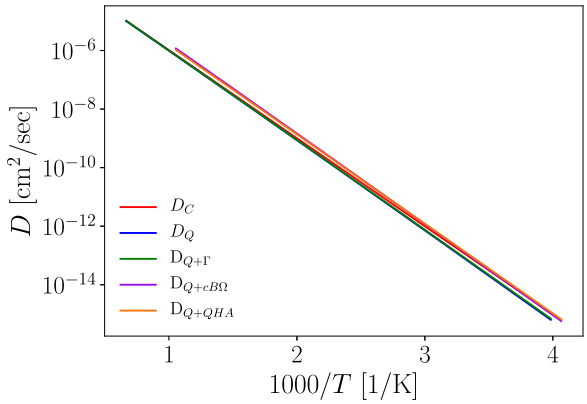

FIG. 16. Temperature dependence of the diffusion coefficient calculated for Li in bulk Si including anharmonic effects. The orange curve shows the diffusion coefficient obtained with QHA, and the purple curve represents the one obtained with the $cB\Omega$ model.

as compared to the equilibrium volume at 0 K. The temperature associated with this volume has been obtained as 853.65 K from the $V(T)$ curve calculated from Ref. 50 (supplementary material). The QHA only includes the explicit volume dependence by means of thermal expansion. Thus, the temperature dependence of ΔE comes from the linear interpolation of the values at 0 K and at an elevated temperature (853 K in this case) using the temperature dependence of the volume curve, as outlined in Eq. (19).

The $cB\Omega$ model includes (approximately) both the explicit volume dependence and the phonon–phonon temperature dependence by employing the temperature dependence of the volume and bulk modulus, respectively. The temperature dependence of the volume and the bulk modulus of silicon was obtained from Refs. 50 and 78 and can be found in the supplementary material. The curves (orange and purple) are adjusted for the ZPE, resulting in a deviation from the value obtained at 0 K without phonon contribution (red filled circle). The $cB\Omega$ model and the QHA differ by about 10 meV in the low temperature regime but stay within ~5 meV–8 meV above 200 K and up to 1000 K, which gives some confidence that both allow us to include the dominating trend due to anharmonic effects. These energy barriers were then used to replace ΔE in Eq. (11) to give the overall temperature dependence of the diffusion coefficients. Figure 16 shows these additional diffusion coefficient curves obtained with the $cB\Omega$ model (purple curve) and with the QHA (orange curve).

At a high temperature, no severe deviation from the Arrhenius equation is observed. This suggests that the anharmonic effects are not very strong. Though, both the approximations show a lateral shift toward higher values of the diffusion coefficient for the entire temperature range. In order to get a better comparison of the two anharmonic models, the ratio of diffusion coefficients is compared to the one obtained with the harmonic approximation (Fig. 17).

The comparative ratios in Fig. 17 show roughly a 60%–70% increase in the diffusion coefficient by including anharmonic effects by means of either model. This increase is more important than the one obtained by including the quantum approximation (~33% in Fig. 8). The $cB\Omega$ model suggests a shift of roughly 70% at a high temperature and tends to stay constant at ~60%. While the QHA shows an initial shift of ~55%, it keeps increasing with temperature as compared to the harmonic approximation.

F. Discussion

The results presented in Secs. III A–III E demonstrate the application of the quantum mechanical framework within the TST framework to study Li diffusion in bulk Si. Moreover, the QHA and the $cB\Omega$ model provide useful insight into the validity of the harmonic approximation. These results are based on several assumptions and approximations: (i) low concentration of the impurity Li atoms, i.e., there is no interaction between the impurity atoms; (ii) the diffusion process is described by the TST framework, assuming every diffusing species that reaches the transition state must also cross it; (iii)

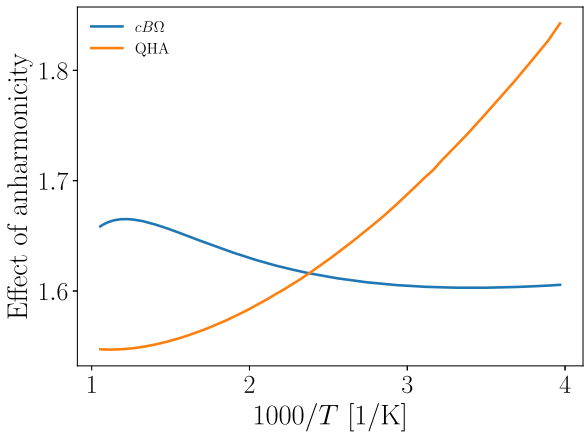

FIG. 17. Temperature dependence of the effect of anharmonicity on the diffusion coefficient measured as a ratio of the diffusion coefficient obtained with the $cB\Omega$ model (blue) and the QHA (orange) with respect to the one obtained with the harmonic approximation (D_Q).

there are no correlated multiple jumps; (iv) only thermally activated incoherent quantum tunneling effects are included and coherent tunneling effects are negligible in the studied temperature range; (v) assessment of anharmonic effects is limited because they depend on the validity of the QHA and the $cB\Omega$ model; and (vi) electronic energies and phonon frequencies for both the ground state and the transition state have been obtained from the DFT with GGA-PBE functional.

Within the framework of these approximations, several effects have been analyzed to estimate the sensitivity of the results, namely, (i) the effect of the quantum mechanical approximation, (ii) the effect of quantum tunneling corrections, (iii) the effect of mass rescaling, and (iv) the effect of anharmonicity. The analysis shows that the diffusion of Li in bulk-Si decreases by roughly 30% by including the quantum mechanical approximation as compared to the classical TST framework.

The decrease in the diffusion coefficient is in agreement with the increase in the effective diffusion barrier as compared to the classical one (refer to Fig. 8). On the other hand, the pre-exponential factor (D^*_{QA}) is slightly higher than the classical one. Globally, the increase in the barrier height dominates and lowers the overall diffusion coefficient as expected in an Arrhenius type equation. The effective diffusion barrier written in Eq. (9) is another form of Eq. (2) that relates the diffusion barrier to the change in the vibrational free energy ΔF^{vib} and a temperature independent term ΔE. Therefore, a higher value of ΔF^{vib}_Q than its classical counterpart increases the diffusion barrier and results in a lower diffusion coefficient. The value of ΔF^{vib}_Q at 0 K corresponds to the ZPE and converges to its classical limit (ΔF^{vib}_C) at a high temperature. However, it is different than simply adding the ZPE to the classical equation because a simple shift rectifies the low temperature limit but overestimates the high temperature limit.[25,79]

The solubility of Li in Si is very low at room temperature,[41,80] which justifies the assumption of low concentration of the diffusing Li atom. Moreover, unless two Li atoms are in the adjacent tetrahedral void (<6 Å apart), there is no effect on the diffusion barrier.[75] Thus, with a supercell with lattice parameters >10 Å, it is safe to assume no interaction between Li atoms in the adjacent cells.

Now, we turn to the discussion of the TST framework for studying diffusion. In the original work of Eyring,[58] a factor c accounts for the recrossing when the activated complex jumps over the barrier and comes back to the initial state without decomposing. This factor is known as the dynamical-correction factor in the literature and decreases the overall diffusion coefficient. It was implicitly set as 1 by Eyring,[58] and later, some researchers have investigated this correction factor and discussed the complexity in estimating its value.[81,82] However, in most of the diffusion studies, it is considered a good assumption to neglect any recrossing, i.e., $c = 1$ is a reasonable approximation.[23,34]

The correlation factor (f) associated with the correlation in multiple jumps is another factor, which is not considered in the present work. The value of this correlation factor is ≤1 and depends on the diffusion mechanism and lattice geometry.[83] Thus, if these correlations are present, it will decrease the diffusion coefficient. Blöchl *et al.*[84] showed that this factor is negligible for H diffusion in Si. Moreover, in the case of dilute interstitial diffusion (as in the present case), the diffusing atom does not have interaction from a neighboring interstitial atom, and thus, there is no correlation between multiple jumps, resulting in $f = 1$.[83] Thus, we can neglect the dynamical-correlation factor in this case without any loss of generality.

Quantum tunneling corrections have been included only by the means of thermally activated incoherent tunneling mechanisms. The coherent tunneling is only active at a very low temperature, near 0 K, and thus has never been observed experimentally, at least for the case of hydrogen.[85,86] Thus, it is safe to neglect it in the temperature range of interest, between 50 K to high temperature.

The only remaining concern is the validation of the harmonic approximation and the applicability of models used to estimate the anharmonicity in the system. With either of the models, the diffusion coefficient increases by 60%–70% as compared to the harmonic approximation. This effect is roughly double than the one observed after including the quantum mechanical effects, which decreased the diffusion coefficient by ~30%. Regarding the accuracy, the QHA estimation of the diffusion constant depends on the precision of NEB calculations and the volume curve. The former was converged until the average energy tolerance was $\leq 1 \times 10^{-5}$ Ha (~27 meV) and the latter had a very good agreement with the experimental data.[50] The $cB\Omega$ model has an additional dependence of bulk modulus, which is a second-order derivative of the volume and can be sensitive to small errors in the volume curve. The literature[33,35] suggests to fit the factor c to the experimental data. However, in the present work, the energy barrier calculated at 0 K is used to adjust c to avoid any accumulation of fitting error. Although it shows a reasonable agreement with the QHA as well as the 0 K NEB results (Fig. 15), it is a simplistic model incorporating both the V and the T dependency without including the phonon–phonon interaction, which might be important at a high temperature.

The GGA-PBE functional that has been used for all the computations slightly overestimates the lattice parameter by <0.7% and shows a very good agreement with the experimental data for the total energy as well as phonon calculations for silicon.[87] In the future, one could perform a comparative study of diffusion coefficients calculated with different functionals.

IV. Li DIFFUSION IN LiSi

A. Crystalline LiSi and Li vacancy effect

Li diffusion in Li_xSi is at least one order of magnitude faster than in bulk Si.[3] LiSi is the first stable crystalline phase in terms of increasing Li:Si ratio and has a higher symmetry (space group: $I4_1/a$) than other Li_xSi phases, with a regular Si network. Three-fold coordinated Si atoms form rings of 8 atoms (S8), as shown by Evers *et al.*,[88] and Li atoms occupy the voids in the chain, as shown in Fig. 18. The Si and Li sublattices are topologically equivalent, forming tetrahedral clusters. The presence of Li atoms distorts the Si network, and the Si–Si bond distance increases from 2.368 Å in bulk Si to 2.418 Å and 2.497 Å, which is in good agreement with the previous first-principles calculations[20] and the experimental data.[44,88] The primitive cell of LiSi consists of 8 Si and 8 Li atoms where each Si atom gets one electron from the Li atom to satisfy the octet rule.[43] The calculated lattice parameters of the fully relaxed primitive LiSi structure studied in this work are $a = b = c = 14.40$ Å with the angles $\alpha = \beta = 99.15°$ and $\gamma = 133°$. The conventional standard structure

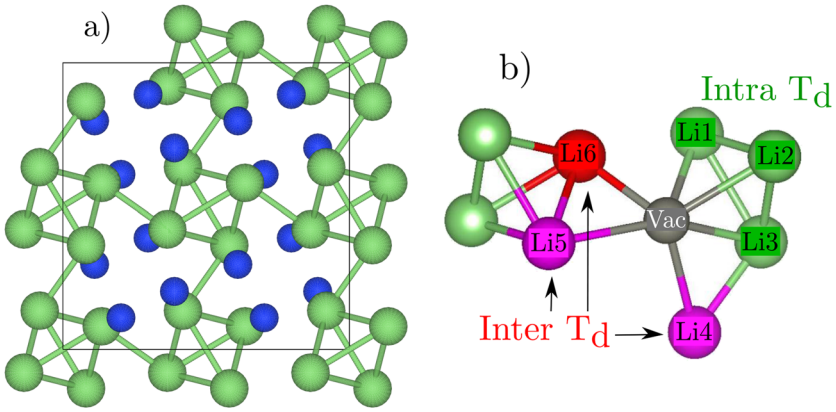

FIG. 18. (a) Conventional unit cell (32 atoms) of the LiSi structure, showing three-fold coordinated Si and tetrahedral Li clusters (Si atoms in blue and Li atoms in green). (b) Zoomed-in image of the same structure centered on one Li vacancy and showing possible jumps to the neighboring Li atoms. Green jumps are intra-tetrahedral jumps, and pink/red jumps are inter-tetrahedral jumps.

contains 16 Si and 16 Li atoms with the lattice parameters $a = b = 9.367$ Å and $c = 5.743$ Å with the angles $\alpha = \beta = \gamma = 90.00°$, which is in good agreement with the experimental XRD data ($a = b = 9.354$ Å, $c = 5.746$ Å) reported by Stearns *et al.*[44]

Four Li atoms in the LiSi structure form a slightly distorted tetrahedron with a Li–Li bond distance of 2.935 Å and 2.944 Å. Each Li atom in this tetrahedral network is connected to three other Li atoms within the same tetrahedra and to three Li atoms (from two other tetrahedra) by three paths (see Fig. 18): one at a distance of 2.683 Å and two at a distance of 3.052 Å (one in each tetrahedron). In total, each Li atom is connected to 6 Li atoms: 3 Li atoms within the same tetrahedron and 3 Li atoms from other tetrahedra, which is consistent with the experimental data.[88]

A previous study by Moon *et al.*[20] has shown that vacancy diffusion is the most energetically favorable mechanism for Li diffusion in LiSi. Since all Wyckoff sites of Li atoms are identical, any Li atom can be removed to create a Li vacancy without losing generality. After removing one Li atom, the volume decreases slightly and the lattice parameter reduces to 14.392 Å (i.e., a decrease of ~0.05%) and angles remain unchanged. Similar to the addition of 1 Li atom in bulk Si, the removal of 1 Li atom from LiSi does not affect much the valence band, except for the removal of two 1s core electrons. The peaks in the conduction band change due to the removal of the 2s electron. Accordingly, in a 16-atom primitive cell, removing a Li atom yields a Fermi energy decrease by 0.62 eV and consequently moves it to the valence band, as shown in Fig. 19. In Sec. IV B, different types of possible vacancy jumps have been studied for calculating the diffusion coefficient.

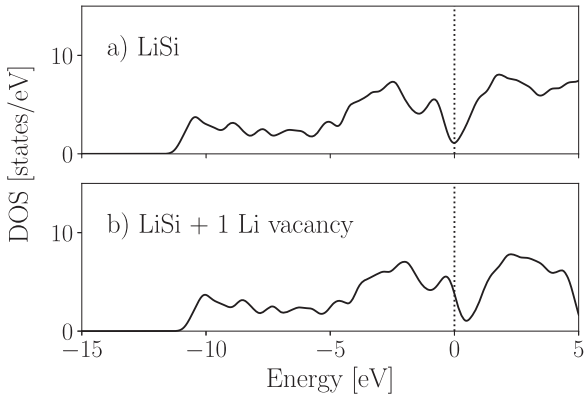

FIG. 19. Electronic density of states of (a) the primitive LiSi cell (16 atoms) with (b) one Li vacancy. The Fermi energy is set to zero on the *x*-axis (dotted line). These small-cell results are shown for illustration purpose only.

B. Migration path and energy barrier

As discussed above, each Li atom can jump to 6 neighboring Li sites within a radial distance of 3.5 Å. Beyond this distance, the calculated migration barriers are very high (>1 eV) and thus will have a negligible contribution in Li diffusion.[20] Out of these 6 jumps, there are 3 intra-T_d jumps (Vac-Li1, Vac-Li2, and Vac-Li3) and 3 inter-T_d ones (Vac-Li4, Vac-Li5, and Vac-Li6) [see Fig. 18(b)]. Out of them, there are 2 pairs of identical jumps: Vac to Li4 and Li5 and Vac to Li1 and Li3 jumps. The remaining two unique jumps are from Vac to Li6 and from Vac to Li2, leaving a total of 4 different types of jumps. The convergence study with respect to the size of the cells was conducted on supercells of the size of 32 atoms (*c*-LiSi), 64 atoms (2 × 1 × 1 of *c*-LiSi), and 128 atoms (2 × 2 × 2 of *p*-LiSi) for individual energy barriers and the overall diffusion coefficient calculated by KMC simulations (see Figs. S2 and S3 of the supplementary material). Although the 64-atom cell was well converged, the biggest supercell of 128 atoms was used in the study for better accuracy. Table I outlines the calculated jump distances and the migration energy barriers for these 4 types of jumps along with

TABLE I. Calculated Li migration jump distances and energy barriers compared with the values reported in the literature.[20]

	Distance (Å)		E_b (eV)	
Jump	This work	Reference 20	This work	Reference 20
Vac-Li1	2.935	2.900	0.247	0.252
Vac-Li2	2.944	2.911	0.261	0.235
Vac-Li4	3.056	3.003	0.430	0.466
Vac-Li6	2.695	2.644	0.252	0.272

the first-principles calculations of Ref. 20. Figure 20 shows the corresponding energy profiles. The agreement is very reasonable given that the present study relies on GGA, while Ref. 20 used the local density approximation (LDA), which is known to underestimate the lattice parameters and hence Li–Li distances. The two types of pathways connecting different tetrahedra are Vac-Li4 and Vac-Li6 with energy barriers of 0.430 eV and 0.252 eV, respectively. In order for Li atoms to diffuse in the LiSi structure, they have to go through one of these inter-tetrahedral paths; therefore, these jumps are rate-limiting. Comparing both energy barriers, the latter is roughly half of the former, and thus, it is more likely to control the effective Li diffusion at room temperature and above.

C. Phonon calculations

Figure 21 shows the vibrational energy calculated from phonon frequencies at the initial and saddle point configurations with the quantum and classical approximations using Eqs. (3) and (4), respectively. As noted in the bulk Si case, the ZPE correction due to the quantum approximation is small and only significant below room temperature. The classical vibrational free energy (F_C^{vib}) goes to zero at 0 K, as shown in Eq. (20), and the limit of the quantum vibrational free energy (F_Q^{vib}) has a finite value, as shown in Eq. (21),

$$\lim_{T\to 0} F_C^{vib} = \lim_{T\to 0} kT \sum_i \ln\left(\frac{h\nu_i}{kT}\right) = 0, \qquad \lim_{T\to 0} \Delta F_C^{vib} = 0, \tag{20}$$

$$\lim_{T\to 0} F_Q^{vib} = \sum_i \left(\frac{h\nu_i}{2}\right), \qquad \lim_{T\to 0} \Delta F_Q^{vib} = \sum_i^{N-1}\left(\frac{h\nu_i^S}{2}\right) - \sum_i^{N}\left(\frac{h\nu_i^0}{2}\right). \tag{21}$$

Instead of only one type of jump in the case of bulk Si, there are six possible vacancy jumps in LiSi. Consequently, there will be six diffusion equations, one for each corresponding jump, and thus, the overall diffusion coefficient cannot be computed directly. Therefore, as mentioned in Sec. II A, a KMC simulation is used to estimate the effective diffusion coefficient due to all these jumps using the DFT data.

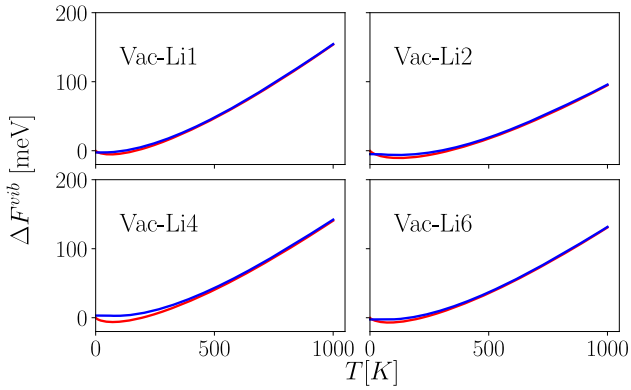

FIG. 21. Temperature dependence of the vibrational free energy for different types of vacancy jumps (refer to Fig. 18 for nomenclature). The red and blue curves indicate the results obtained using the classical and quantum approximations, respectively.

D. Effective diffusion coefficient: KMC

KMC simulations were performed on a conventional LiSi lattice with a single Li vacancy through which Li atoms will diffuse with the above calculated energy barriers. The diffusion coefficient for each one of the six jumps was calculated with the quantum and classical approximations using Eqs. (5) and (6). Similar to bulk Si, the quantum tunneling correction shows a very small effect on the diffusion coefficient near room temperature. The ratio of $D_{Q+\Gamma}/D_Q$ for all four jumps (Fig. S4 of the supplementary material) is less than 1.05 (i.e., less than 5% change) near room temperature, and it increases for lower temperature. However, unlike bulk Si, the overall diffusion coefficient of Li in LiSi is calculated at discrete temperature values, which are at or above room temperature. Moreover, we have already shown in Sec. III D that the heavy mass of Li, as compared to H, significantly diminishes the quantum effect. Thus, it was safe to ignore the quantum tunneling corrections in the KMC study for the LiSi case.

Figure 22 shows the distribution of the diffusion coefficients D_i obtained from KMC simulations at different temperatures from 40 000 sites with 10 000 steps each based on the jump rates determined from the classical approximation. Because the selection of an

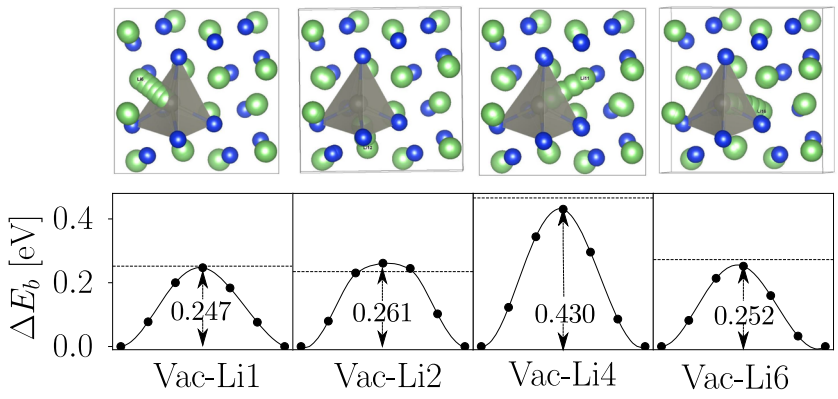

FIG. 20. Four types of Li vacancy jumps (above) and associated minimum energy pathways (below). Gray shaded area shows the tetrahedral polyhedra around the initial Li vacancy site. The energy barrier height is indicated by the peak height inside the graph (in eV) (refer to Fig. 18 and Table I for the nomenclature associated with the type of jump). The horizontal dashed line indicates the value reported in Ref. 20.

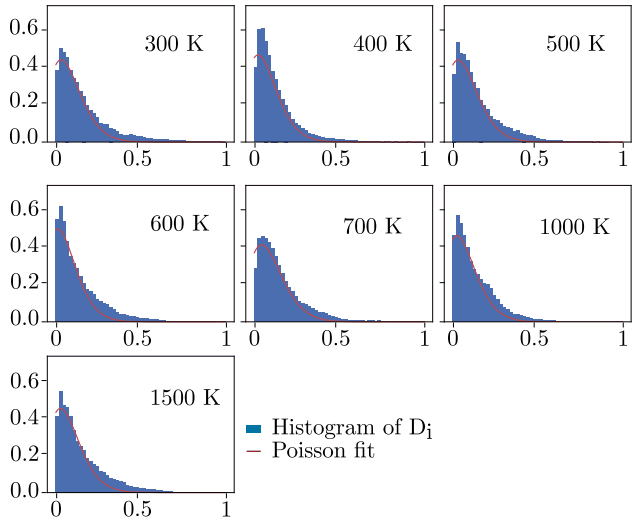

FIG. 22. Statistics showing the distribution of the diffusion coefficients (D_i for each of the 40 000 runs) obtained from KMC simulation for each temperature. The solid line (red) is obtained by fitting a Poisson distribution. The data are normalized [$|D_i| = D_i/\max(D_i)$] and binned into 50 bins for curve fitting over the distribution. The *y*-axis represents the probability of the Poisson distribution.

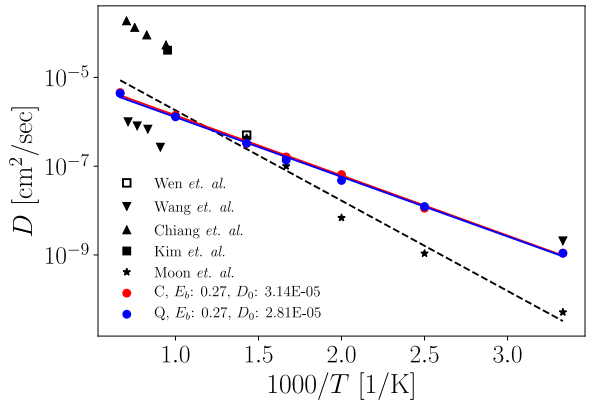

FIG. 23. Temperature dependence of the effective diffusion coefficient (D) obtained from KMC simulation. Dots in red and blue indicate values obtained with classical and quantum approximations of attempt frequencies, respectively. Solid lines show the fitted Arrhenius plot to get the effective pre-factor and the effective energy barrier. The experimental data point is shown by the empty square (black), and results from previous theoretical investigations[3,14,16,17,20] are indicated by filled markers (black).

event in the KMC algorithm gives a Poisson distribution,[54] we also show a Poisson distribution fit (red curve) as a guide for the eye. The good agreement between the distribution obtained from the KMC study (histograms) and the Poisson fit (red curve) suggests that the KMC simulations provide sufficiently converged results.

The effective diffusion coefficient of this distribution has been calculated by using Eq. (B5), as suggested in Refs. 54 and 59. Similarly, an effective diffusion coefficient was also calculated based on the jump rate calculated from the quantum approximation. Figure 23 shows the Arrhenius fit for these values obtained for the classical and quantum approximations, and a comparison with the experimental data[3] and previous KMC simulations performed by Moon *et al.*[20] Due to the scarcity of experimental data for the LiSi phase, the diffusion data from Wen and Huggins[3] on other Li_xSi phases were used as a rough estimate for the diffusion of Li in LiSi; Moon *et al.*[20] also used the same reference.

The diffusion coefficients obtained from both approximations provide a good fit for the Arrhenius equation with an effective barrier of 0.27 eV and a diffusion pre-factor of 2.81×10^{-5} cm^2/s $\pm$ 0.5 $\times 10^{-5}$ cm^2/s. Quantum effects have a marginal role in the diffusion coefficient of Li in LiSi, providing the same diffusion barrier of 0.27 eV and a prefactor of 3.14×10^{-5} cm^2/s. The diffusion coefficients obtained from both approximations are in close agreement with the experimental data[3] at 700 K. The filled markers in the plot represent other theoretical values of the diffusion coefficients obtained from *ab initio* molecular dynamics studies at high temperatures.

E. Effect of anharmonicity

Similar to the bulk Si case, the effect of anharmonicity on the diffusion of Li in LiSi is studied by the means of QHA and the $cB\Omega$ model using the temperature-dependent volume and bulk modulus. Figures 24 and 25 show these quantities calculated from first principles.

Because of the slow kinetics of formation, the LiSi phase is difficult to form at room temperature and normal pressure (NP), and thus, there are limited experimental data on its structural properties.[41,44] Stearns *et al.*[44] have synthesized c-LiSi in laboratory at a high temperature and high pressure (HP), and reported a volume of 15.75 Å^3/atom from x-ray diffraction data by Rietveld refinement. Our ZPE corrected volume at zero temperature (15.83 Å^3/atom) is 0.08 Å^3/atom higher than their value, as shown in Fig. 24. However, at the time of writing, we are not aware of any experimental data for elastic properties of the c-LiSi phase.

A previous DFT calculation (with the LDA functional) by Taubert *et al.*[89] has reported a value of 56.8 GPa for the bulk modulus of LiSi at zero temperature, which is in good agreement (±10%)

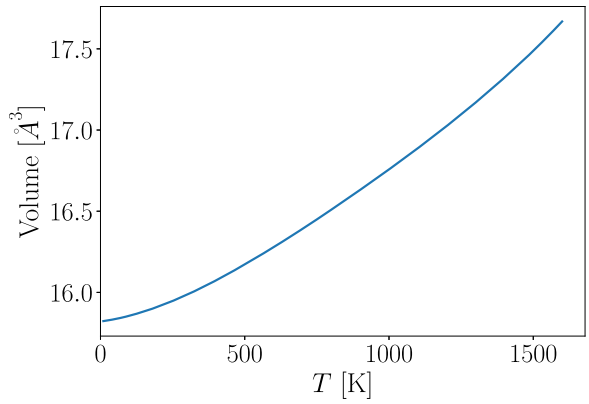

FIG. 24. Temperature dependence of the LiSi primitive volume from first principles.

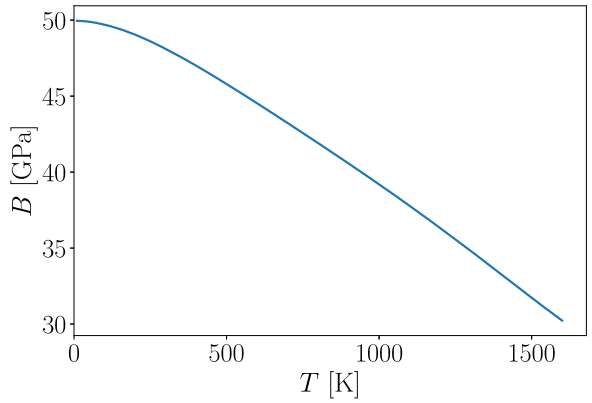

FIG. 25. Temperature dependence of the LiSi bulk modulus from first principles.

with the value of 50 GPa calculated in this study (Fig. 25). Moreover, there is a well-established general tendency of GGA-PBE to underestimate the bulk modulus,[90] while LDA can present errors of both signs, i.e., higher and lower.[87]

Figure 26 shows the temperature dependence of the diffusion barriers for all four types of vacancy jumps calculated with the $cB\Omega$ model and the QHA according to Eqs. (16) and (19), respectively. The $cB\Omega$ model shows the same overall trend for all four jumps as expected. The temperature varying ingredient, the volume per unit atom (Ω) and the bulk modulus, remains the same for all four types of jumps, thus resulting in the same curve scaled to a different energy level corresponding to each jump.

The overall decreasing trend is due to the lattice softening with the thermal expansion, which in most cases decreases the diffusion barrier. This ability of the $cB\Omega$ model to incorporate the anharmonic effects in a simple model by means of volume and bulk modulus makes it a promising approach to study anharmonicity and has shown good results in studying diffusion in several semiconductors and metal oxides.[37] However, in the case of the Vac-Li1 jump, according to the QHA, the diffusion barrier increases with temperature. Thus, the $cB\Omega$ model and the QHA approach diverge for this case. The QHA uses an additional information about the diffusion barrier at an elevated temperature (920 K in this case), and thus, it treats more accurately the volume dependence, but the lack of treatment of the phonon–phonon interaction prevents us to conclude that it is better than the $cB\Omega$ model, as already outlined. We can simply note that while both approaches agree on the decrease in the barrier energy with temperature for three out of four types of jumps, they disagree for the Vac-Li1 jump. Similar to what was done in the harmonic approximation, the KMC simulation was used to calculate the effective diffusion coefficient for the Li vacancy jump for both the models to study the anharmonic effects.

Figure 27 shows the effective diffusion coefficients obtained with the KMC simulation at discrete temperatures using the individual vacancy diffusion coefficient calculated with the $cB\Omega$ model (violet) and the QHA (orange). The individual points fit very well with the Arrhenius equation with a R^2 value of 0.99 in all the cases. The corresponding values of diffusion pre-factor D_0 and the diffusion barrier E_b are within an error range of $\pm 0.6 \times 10^{-5}$ and ± 0.01 eV, respectively. Both the approximations show a slight increase in the diffusion coefficient at a high temperature due to anharmonic effects with a slightly higher slope (0.28 eV) as compared to the harmonic approximation (0.27 eV). However, the difference is within the error limits of the KMC simulation.

In order to have a better comparison, the effective diffusion coefficients from both approximations are shown in Fig. 28 as a ratio with respect to the harmonic approximation with quantum mechanical corrections (D_Q). The effect of quantum mechanical corrections is also shown on the secondary axis as the ratio of D_Q vs D_C for comparison.

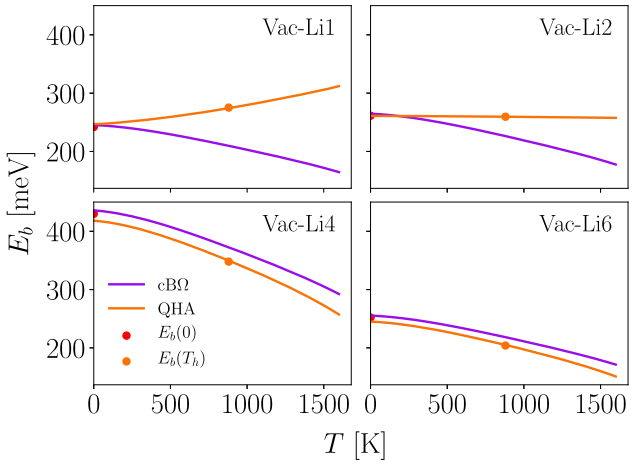

FIG. 26. Temperature dependence of the diffusion energy barrier calculated with the $cB\Omega$ model (violet) and with the QHA (orange) for all four types of jumps. Red and orange dots are the values obtained from NEB calculations at 0 K and 920 K, respectively.

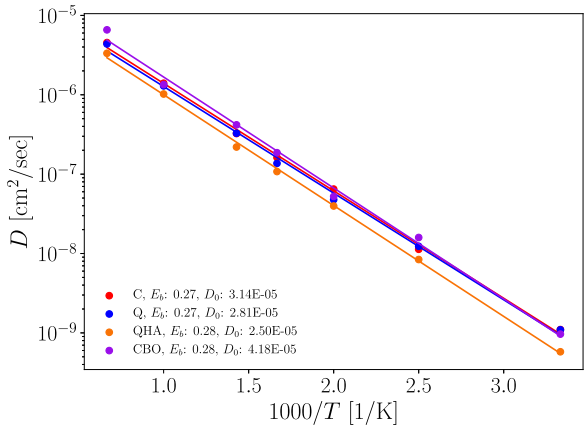

FIG. 27. Temperature dependence of the Li diffusion coefficient in LiSi obtained from the KMC simulations. The harmonic classical (red) and quantum (blue) approximations are shown along with the $cB\Omega$ model (violet) and with the QHA (orange) to study anharmonicity in the system. The error (variance) in the values of E_b and D_0 is ± 0.01 eV and $\pm 0.6 \times 10^{-5}$, respectively.

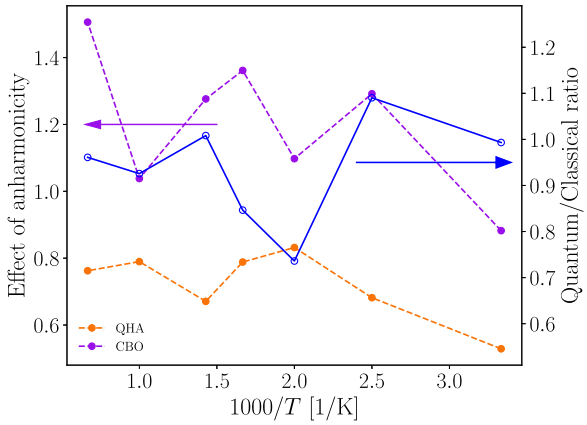

FIG. 28. The effect of anharmonicity is shown as a ratio of the diffusion coefficient obtained with the QHA (orange) and the $cB\Omega$ model (violet) with respect to the one obtained with the harmonic approximation (D_Q) at each temperature using KMC. The ratio of D_Q/D_C is also shown on the secondary axis with the same scale for comparison.

F. Discussion

In this subsection, all the results obtained for Li diffusion in LiSi via the vacancy mechanism are discussed and compared with the reported literature. The values of the effective diffusion coefficient obtained in the KMC study are in good agreement with the experimental data at 700 K[3] (see Fig. 23). In a previous KMC study, Moon *et al.*[20] also reported a similar value at 700 K. However, their low temperature diffusivity values are at least one order of magnitude smaller than our results. The least square fit of their reported values gives an effective barrier of 0.40 eV. Nonetheless, they reported an effective barrier of 0.306 eV for Li diffusion in LiSi, which is close to the value obtained in our study (0.27 eV ± 0.01 eV). Moreover, an effective barrier of 0.40 eV is much higher than the smallest inter-T_d barrier of 0.27 eV and close to the higher energy inter-T_d jumps (0.47 eV) (refer to Table I). These high-energy jumps are unlikely to contribute significantly at room temperature, and thus, the effective barrier should be close to the smallest one and not to the largest one. The discrepancy can be due to insufficient statistics of the KMC calculation and error bars.

AIMD studies conducted by Chiang *et al.*[16] reported a higher diffusion coefficient (filled triangle) of the order of 10^{-4} cm^2/s with an effective barrier of 0.38 eV in the high temperature range. It is one order of magnitude higher than the values reported in this study. Their extrapolated value at 700 K is also roughly an order of magnitude higher than the experimental data. A similar AIMD study by Kim *et al.*[17] (filled square) also showed a similar value of diffusion coefficient at 1050 K. However, both these studies were performed with the liquid LiSi phase, in which diffusion is expected to be slightly higher than the corresponding solid phase. Thus, the room temperature extrapolation is not an accurate description of diffusion in the c-LiSi phase.

In another study, Wang *et al.*[14] calculated the Li diffusion coefficient (upside down filled triangle) during lithiation of Si to form LiSi in a similar temperature range. However, unlike Chiang *et al.*,[16] they started with the room-temperature structure of solid Si to form LiSi, instead of a liquid/amorphous one. Their reported values are in better agreement with the experimental data, and their room temperature value is also in close agreement with our results. The discrepancy in the abovementioned two sets of AIMD studies carried out in a similar temperature range shows roughly a difference of 2 orders of magnitude between the solid and liquid LiSi phases, and thus, one has to be careful about the phase while doing the AIMD studies at elevated temperatures.

Comparing KMC simulations with MD, apart from the advantages of studying low temperature/slow processes, one of the disadvantages is the explicit inclusion of anharmonicity, while MD implicitly includes it. Moreover, the accuracy of KMC studies relies on the completeness or convergence of diffusion events and the accuracy of the energy barriers. In this study, both the parameters were carefully monitored for convergence, i.e., convergence of diffusion events to a Poisson distribution for the former (see Fig. 22) and a varying supercell study for the latter (see the supplementary material). Future experimental results can further validate the accuracy of these KMC results.

Regarding the validation of the harmonic approximation in the LiSi case (refer to Fig. 28), both approximations ($cB\Omega$ model and QHA) separate at a high temperature (except at 1000 K). For instance, the $cB\Omega$ model increases the diffusion coefficient, while the QHA decreases it. The difference in the two approximations might be due to the discrepancy in the estimated diffusion barrier for one of the four inter-tetrahedral jumps (Vac-Li1), as shown in Fig. 26. On the one hand, the QHA can underestimate the anharmonicity as it does not include the phonon–phonon interaction that can play a significant role at a high temperature.[32,49] On the other hand, the $cB\Omega$ model relies on the temperature-dependent bulk modulus and thermal expansion, and with a lack of experimental data, its validity is not clear. Although, in the low temperature range, the overall trend from both the approximations shows an increase in the diffusion coefficient with an increase in temperature, none of them provide a convincing proof of having significant anharmonic effects on the diffusion of Li in LiSi.

V. CONCLUSION

In this study, we have performed a first-principles based study of Li diffusion in bulk Si and c-LiSi phases within the transition state theory framework and also taking into account nuclear quantum approximations and anharmonic effects. As compared to the classical approach, the addition of quantum effects for Li diffusion in Si lowers the value of the room temperature diffusion coefficient by 33% because of a higher effective energy barrier. The $cB\Omega$ model and the quasi-harmonic approximation suggest an increase in the diffusion coefficient by 60% in the case of bulk Si by including anharmonic effects. However, they fail to give a compelling evidence of significant anharmonic effects in the case of LiSi. Based on these findings, we propose that the nuclear quantum effects and anharmonic effects are rather weak and only play a marginal role in the Li–Si system.

The obtained results are in good agreement with previous experimental and theoretical studies. For Li diffusion in bulk Si, we obtained an energy barrier of 0.59 eV with a diffusion pre-factor of 1×10^{-3} cm^2/s. In the case of LiSi, our calculations are in better

agreement with the experimental data than previous *ab initio* molecular dynamics studies conducted at higher temperatures. We obtained an effective diffusion barrier of 0.27 eV ± 0.01 eV with a pre-factor of 2.8 ± 1.1 × 10^{-5} cm^2/s for Li diffusion in LiSi. Moreover, we propose that one of the inter-tetrahedral jumps with an energy barrier of 0.25 eV is the rate-limiting step for long range Li diffusion in LiSi.

The main advantages of using the current approach over molecular dynamics are the following: (1) unlike molecular dynamics, this approach can be used for slow diffusion processes near room temperature and (2) it gives a better understanding of the different diffusion mechanisms involved, and thus, it is helpful in designing new materials with the desired diffusion properties. This makes it a potential approach in studying even more complex systems, for instance, Li diffusion in lithiated Li_xSi phases with defects. Based on our results, this approach can be used in studying room temperature Li diffusion in different anode materials and can possibly increase our understanding in designing next-generation batteries.

SUPPLEMENTARY MATERIAL

The supplementary material contains convergence tests for the supercell size, bulk modulus, and volume change of bulk-Si used to study anharmonic effects as well as the phonon band structure of c-LiSi and with 1 Li atom vacancy.

ACKNOWLEDGMENTS

The authors acknowledge technical help from J.-M. Beuken and M. Giantomassi. This work was supported by the Communauté française de Belgique through the BATTAB Project (No. ARC 14/19–057) and the Région Wallone through the BATWAL Project (No. 1318146). Computational resources have been provided by the supercomputing facilities of the Université Catholique de Louvain (CISM/UCL) and the Consortium des Equipements de Calcul Intensif en Fédération Wallonie Bruxelles (CÉCI) funded by the Fond de la Recherche Scientifique de Belgique (F.R.S.-FNRS) under convention No. 2.5020.11. The present research benefited from computational resources made available on the Tier-1 supercomputer of the Fédération Wallonie-Bruxelles, infrastructure funded by the Walloon Region under Grant Agreement No. 1117545.

APPENDIX A: HARMONIC APPROXIMATION

The free energy can be expressed in terms of the partition function $Z(T)$ using Boltzmann statistics,[46]

$$F(T) = -kT \ln Z(T). \tag{A1}$$

Assuming harmonic approximation for the lattice vibrations, the partition function can be written in terms of the vibrational frequencies (ν_i) and the ground-state energy (E_0) using the quantum mechanical expressions,[46]

$$Z(T) = e^{-E_0/kT} \prod_i \frac{1}{2\sinh\left(\frac{h\nu_i}{2kT}\right)} \tag{A2}$$

$$\Rightarrow F(T) = -kT \ln\left(e^{-E_0/kT} \prod_i \frac{1}{2\sinh\left(\frac{h\nu_i}{2kT}\right)}\right)$$

$$= E_0 + kT \sum_i \ln\left[2\sinh\left(\frac{h\nu_i}{2kT}\right)\right], \tag{A3}$$

where ν_i is the vibrational frequency of the ith mode with $h\nu_i$ being the quantum of energy of the harmonic oscillator. The second term in Eq. (A3) can be written as the vibrational free energy (F_Q^{vib}),[24]

$$F_Q^{vib}(T) = kT \sum_i \ln\left\{2\sinh\frac{h\nu_i}{2kT}\right\} \tag{A4}$$

$$= \sum_i \left\{\frac{1}{2}h\nu_i + kT \ln\left[1 - e^{-h\nu_i/kT}\right]\right\}. \tag{A5}$$

The classical limit of this expression is given by[24]

$$F_C^{vib}(T) = kT \sum_i \ln\left(\frac{h\nu_i}{kT}\right). \tag{A6}$$

APPENDIX B: KMC ALGORITHM

The main steps of the KMC algorithm are as follows:

Step 1: Identify all the events (q) that can take place in the current atomic configuration.

Step 2: Determine rates (k_i) of all possible events. The jump rate τ_i for an event i is given by the transition state theory[45,58] as

$$\tau_i = \gamma_i e^{-\Delta E_i/kT}, \tag{B1}$$

where γ_i is the attempt frequency, ΔE_i is the energy barrier, k is the Boltzmann constant, and T is the temperature associated with event i. For all the events, the attempt frequency was calculated using the phonon vibration modes and energy barriers by the NEB method. For the classical approximation, the attempt frequency (γ_i) is the ratio of phonon frequencies for the initial and saddle points within the classical transition state theory framework and is temperature invariant. For the quantum approximation, it varies with temperature and is given by

$$\gamma_i = \frac{kT}{h} \frac{\prod_{i=1}^{N} 2\sinh\left(\frac{h\nu_i^0}{2kT}\right)}{\prod_{i=1}^{N-1} 2\sinh\left(\frac{h\nu_i^S}{2kT}\right)}. \tag{B2}$$

Step 3: Generate a uniform random number between 0 and 1 (r_1) to select the event p out of all the q events to take place as

$$\sum_{i=1}^{p-1} k_i < r_1 k_{tot} \le \sum_{i=1}^{p} k_i, \tag{B3}$$

where k_{tot} is the cumulative sum of rates of all the possible events.

Step 4: Reconfigure the system according to the selected event.

Step 5: Since selecting an event randomly is a type of Poisson process, the time evolution for each KMC step can be evaluated as[91]

$$t \to t - \ln(r_2)/k_{tot}, \tag{B4}$$

where r_2 is a second random number between 0 and 1.

Step 6: Update new positions of Li atoms and vacancy, and update the time according to step 5.
Step 7: Return to step 1.

Repeat this process for a sufficiently large number of times. The diffusion coefficient can then be calculated as the time-weighted average of the diffusion coefficients for each site i,[61]

$$D = \sum_i D_i \Delta t_i / t, \tag{B5}$$

where D_i is the diffusion coefficient calculated for each site i over time Δt_i and t is the total time for the entire KMC simulation, and the expression

$$D_i = \langle [r(t_i) - r(t_0)]^2 \rangle / 2d\Delta t_i \tag{B6}$$

gives the diffusion coefficient of each site i. The vectors $r(t_i)$ and $r(t_0)$ represent the final and initial positions of the vacancy, respectively. The variable d denotes the dimensions of the simulation, and $\langle \ldots \rangle$ denotes the average over all particles.

DATA AVAILABILITY

The data that support the findings of this study are available from the corresponding author upon reasonable request.

REFERENCES

[1] C.-M. Park, J.-H. Kim, H. Kim, and H.-J. Sohn, Chem. Soc. Rev. **39**, 3115 (2010).
[2] L. Y. Beaulieu, K. W. Eberman, R. L. Turner, L. J. Krause, and J. R. Dahn, Electrochem. Solid-State Lett. **4**, A137 (2001).
[3] C. J. Wen and R. A. Huggins, J. Solid State Chem. **37**, 271 (1981).
[4] B. Key, R. Bhattacharyya, M. Morcrette, V. Seznec, J.-M. Tarascon, and C. P. Grey, J. Am. Chem. Soc. **131**, 9239 (2009).
[5] N. Balke, S. Jesse, Y. Kim, L. Adamczyk, A. Tselev, I. N. Ivanov, N. J. Dudney, and S. V. Kalinin, Nano Lett. **10**, 3420 (2010).
[6] N. Ding, J. Xu, Y. X. Yao, G. Wegner, X. Fang, C. H. Chen, and I. Lieberwirth, Solid State Ionics **180**, 222 (2009).
[7] A. Kuhn, P. Sreeraj, R. Pöttgen, H.-d. Wiemhöfer, M. Wilkening, P. Heitjans, H. D. Wiemhofer, M. Wilkening, and P. Heitjans, J. Am. Chem. Soc. **133**, 11018 (2011).
[8] K. Yoshimura, J. Suzuki, K. Sekine, and T. Takamura, J. Power Sources **174**, 653 (2007).
[9] W. Wan, Q. Zhang, Y. Cui, and E. Wang, J. Phys.: Condens. Matter **22**, 415501 (2010).
[10] G. A. Tritsaris, K. Zhao, O. U. Okeke, and E. Kaxiras, J. Phys. Chem. C **116**, 22212 (2012).
[11] H. Kim, K. E. Kweon, C. Y. Chou, J. G. Ekerdt, and G. S. Hwang, J. Phys. Chem. C **114**, 17954 (2010).
[12] E. M. Pell, Phys. Rev. **119**, 1014 (1960).
[13] D. Di Stefano *et al.*, Chem **5**, 2450 (2019); arxiv:1708.02997.
[14] Z. Wang, Q. Su, H. Deng, and Y. Fu, ChemElectroChem **2**, 1292 (2015).
[15] Z. Wang, Q. Su, H. Deng, W. He, J. Lin, and Y. Q. Fu, J. Mater. Chem. A **2**, 13976 (2014).
[16] H.-H. Chiang, J.-M. Lu, and C.-L. Kuo, J. Chem. Phys. **144**, 034502 (2016).
[17] H. Kim, C.-Y. Chou, J. G. Ekerdt, and G. S. Hwang, J. Phys. Chem. C **115**, 2514 (2011).
[18] P. Johari, Y. Qi, and V. B. Shenoy, Nano Lett. **11**, 5494 (2011).
[19] S. Zheng and J. Pfaendtner, Mol. Simul. **41**, 55 (2015).
[20] J. Moon, B. Lee, M. Cho, and K. Cho, J. Power Sources **328**, 558 (2016).
[21] M. Ceriotti, G. Miceli, A. Pietropaolo, D. Colognesi, A. Nale, M. Catti, M. Bernasconi, and M. Parrinello, Phys. Rev. B **82**, 174306 (2010).
[22] G. J. Ackland, M. Dunuwille, M. Martinez-Canales, I. Loa, R. Zhang, S. Sinogeikin, W. Cai, and S. Deemyad, Science **356**, 1254 (2017).
[23] M. Dixit, H. Engel, R. Eitan, D. Aurbach, M. D. Levi, M. Kosa, and D. T. Major, J. Phys. Chem. C **119**, 15801 (2015).
[24] K. Toyoura, Y. Koyama, A. Kuwabara, F. Oba, and I. Tanaka, Phys. Rev. B **78**, 214303 (2008).
[25] D. Di Stefano, M. Mrovec, and C. Elsässer, Phys. Rev. B **92**, 224301 (2015).
[26] C. O. Hwang, J. Chem. Phys. **125**, 226101 (2006).
[27] N. Sandberg, B. Magyari-Köpe, and T. R. Mattsson, Phys. Rev. Lett. **89**, 065901 (2002).
[28] M. Mantina, Y. Wang, R. Arroyave, L. Q. Chen, Z. K. Liu, and C. Wolverton, Phys. Rev. Lett. **100**, 215901 (2008).
[29] D. Zhao, Y. Kong, A. Wang, L. Zhou, S. Cui, X. Yuan, L. Zhang, and Y. Du, J. Phase Equilib. Diffus. **32**, 128 (2011).
[30] C. P. Flynn, Z. Naturforsch., A **26**, 99 (1971).
[31] G. DeLorenzi, C. P. Flynn, and G. Jacucci, Phys. Rev. B **30**, 5430 (1984).
[32] D. S. Kim, H. L. Smith, J. L. Niedziela, C. W. Li, D. L. Abernathy, and B. Fultz, Phys. Rev. B **91**, 014307 (2015).
[33] V. Saltas, A. Chroneos, and F. Vallianatos, J. Mater. Sci.: Mater. Electron. **29**, 12022 (2018).
[34] E. Wimmer, W. Wolf, J. Sticht, P. Saxe, C. B. Geller, R. Najafabadi, and G. A. Young, Phys. Rev. B **77**, 134305 (2008).
[35] P. Varotsos and K. Alexopoulos, Phys. Rev. B **15**, 4111 (1977).
[36] P. Varotsos, W. Ludwig, and K. Alexopoulos, Phys. Rev. B **18**, 2683 (1978).
[37] A. Chroneos, Appl. Phys. Rev. **3**, 041304 (2016).
[38] C. Wert and C. Zener, Phys. Rev. **76**, 1169 (1949).
[39] P. Varotsos, J. Appl. Phys. **101**, 123503 (2007).
[40] H. Okamoto, J. Phase Equilib. Diffus. **30**, 118 (2009).
[41] M. H. Braga, A. Dębski, and W. Gąsior, J. Alloys Compd. **616**, 581 (2014).
[42] V. L. Chevrier, J. W. Zwanziger, and J. R. Dahn, Can. J. Phys. **87**, 625 (2009).
[43] V. L. Chevrier, J. W. Zwanziger, and J. R. Dahn, J. Alloys Compd. **496**, 25 (2010).
[44] L. A. Stearns, J. Gryko, J. Diefenbacher, G. K. Ramachandran, and P. F. McMillan, J. Solid State Chem. **173**, 251 (2003).
[45] G. H. Vineyard, J. Phys. Chem. Solids **3**, 121 (1957).
[46] M. Born and H. Kuang, in *Dynamical Theory of Crystal Lattices* (Clarendon, Oxford, 1962), Chap. 4, p. 166.
[47] J. T. Fermann and S. Auerbach, J. Chem. Phys. **112**, 6787 (2000).
[48] A. Fleszar and X. Gonze, Phys. Rev. Lett. **64**, 2961 (1990).
[49] P. Pavone, K. Karch, O. Schütt, D. Strauch, W. Windl, P. Giannozzi, and S. Baroni, Phys. Rev. B **48**, 3156 (1993).
[50] G.-M. Rignanese, J.-P. Michenaud, and X. Gonze, Phys. Rev. B **53**, 4488 (1996).
[51] P. Varotsos and K. Alexopoulos, Phys. Rev. B **30**, 7305 (1984).
[52] G. Henkelman and H. Jónsson, J. Chem. Phys. **113**, 9978 (2000).
[53] G. Henkelman, B. P. Uberuaga, H. Jónsson, G. Henkelman, and H. Jo, J. Chem. Phys. **113**, 9901 (2000).
[54] Y. A. Du, J. Rogal, and R. Drautz, Phys. Rev. B **86**, 174110 (2012).
[55] T. Vegge, Phys. Rev. B **70**, 035412 (2004).
[56] A. B. Bortz, M. H. Kalos, and J. L. Lebowitz, J. Comput. Phys. **17**, 10 (1975).
[57] D. T. Gillespie, J. Comput. Phys. **22**, 403 (1976).
[58] H. Eyring, J. Chem. Phys. **3**, 107 (1935).
[59] R. Kirchheim, Acta Metall. **35**, 271 (1987).
[60] R. Kirchheim, Prog. Mater. Sci. **32**, 261 (1988).
[61] A. Ramasubramaniam, M. Itakura, M. Ortiz, and E. A. Carter, J. Mater. Res. **23**, 2757 (2008).
[62] X. Gonze *et al.*, Comput. Mater. Sci. **25**, 478 (2002).
[63] X. Gonze *et al.*, Z. Kristallogr. **220**, 558 (2005).
[64] X. Gonze *et al.*, Comput. Phys. Commun. **180**, 2582 (2009).

[65]X. Gonze *et al.*, Comput. Phys. Commun. **205**, 106 (2016).
[66]J. P. Perdew, K. Burke, and M. Ernzerhof, Phys. Rev. Lett. **77**, 3865 (1996).
[67]D. R. Hamann, Phys. Rev. B **88**, 085117 (2013).
[68]M. J. van Setten, M. Giantomassi, E. Bousquet, M. J. Verstraete, D. R. Hamann, X. Gonze, and G.-M. Rignanese, Comput. Phys. Commun. **226**, 39 (2018).
[69]M. Methfessel and A. T. Paxton, Phys. Rev. B **40**, 3616 (1989).
[70]Q. Zhang, W. Zhang, W. Wan, Y. Cui, and E. Wang, Nano Lett. **10**, 3243 (2010).
[71]X. Gonze, Phys. Rev. B **55**, 10337 (1997).
[72]X. Gonze and C. Lee, Phys. Rev. B **55**, 10355 (1997).
[73]R. Caracas, G.-M. Rignanese, and X. Gonze, Z. Kristallogr. **220**, 458 (2005).
[74]F. D. Murnaghan, Proc. Natl. Acad. Sci. U. S. A. **30**, 244 (1944).
[75]J. Moon, B. Lee, M. Cho, and K. Cho, J. Power Sources **272**, 1010 (2014).
[76]A. S. Fedorov, Z. I. Popov, A. A. Kuzubov, and S. G. Ovchinnikov, JETP Lett. **95**, 143 (2012).
[77]E. M. Pell, Phys. Rev. **119**, 1222 (1960).
[78]S. Rajagopalan, Nuovo Cimento B Ser. **51**, 222 (1979).
[79]D. E. Jiang and E. A. Carter, Phys. Rev. B **70**, 064102 (2004).
[80]A. G. Morachevskii and A. I. Demidov, Russ. J. Appl. Chem. **88**, 547 (2015).
[81]A. F. Voter, Phys. Rev. Lett. **63**, 167 (1989).
[82]G. A. Voth, J. Phys. Chem. **97**, 8365 (1993).
[83]H. Mehrer, in *Diffusion in Solids* (Springer, Berlin, Heidelberg, 2007), Chap. 7, pp. 105–125.
[84]P. E. Blöchl, C. G. Van de Walle, and S. T. Pantelides, Phys. Rev. Lett. **64**, 1401 (1990).
[85]H. Grabert and H. R. Schober, in *Hydrogen in Metals III*, edited by H. Wipf (Springer, Berlin, Heidelberg, 1997), Chap. 2.
[86]D. Di Stefano, "First-principles investigation of hydrogen interaction with metals," Ph.D. thesis, Albert-Ludwigs-Universitat Frieburg, 2016.
[87]L. He, F. Liu, G. Hautier, M. J. T. Oliveira, M. A. L. Marques, F. D. Vila, J. J. Rehr, G. M. Rignanese, and A. Zhou, Phys. Rev. B **89**, 064305 (2014).
[88]J. r. Evers, G. Oehlinger, and G. Sextl, Angew. Chem., Int. Ed. Engl. **32**, 1442 (1993).
[89]F. Taubert, S. Schwalbe, J. Seidel, R. Hüttl, T. Gruber, R. Janot, M. Bobnar, R. Gumeniuk, F. Mertens, and J. Kortus, Int. J. Mater. Res. **108**, 942 (2017).
[90]K. Lejaeghere, V. Van Speybroeck, G. Van Oost, and S. Cottenier, Crit. Rev. Solid State Mater. Sci. **39**, 1 (2014).
[91]K. A. Fichthorn and W. H. Weinberg, J. Chem. Phys. **95**, 1090 (1991).